

POLITECNICO DI TORINO
Master's Degree in Mechatronic's Engineering



Master's Degree Thesis
**State of Charge and parameter
estimation for a 48V Lithium-Ion battery
based on temperature dependent
second-order RC model**

Supervisors

Prof. Angelo BONFITTO

Phd. Sara LUCIANI

Phd. Pier Giuseppe ANSELMA

Candidate

Leonardo PASQUALI

July 2022

Summary

As part of the midterm evaluation of the 2022-2025 Light-Duty Vehicle Greenhouse Gas (GHG) Standards, the U.S. Environmental Protection Agency (EPA) developed simulation models for studying the effectiveness of 48V mild hybrid electric vehicle (MHEV) technology for reducing CO_2 emissions from light-duty vehicles. Simulation and modeling of this technology requires a suitable model of the battery.

The goal of this thesis work is to define an equivalent model of a lithium-ion battery ($LiFePO_4$) 48V for mild hybrid applications, which is able to correctly simulate its behavior. The battery model is a standard equivalent circuit model with the two-time constant resistance-capacitance (RC) blocks. Resistances and capacitances were modeled using lookup tables, allowing flexibility for the model, to closely match measured data. Pulse discharge curves and charge curves are collected experimentally to characterize the battery performance at various operating points depending on state of charge and temperature. It can be extremely difficult to fit the simulation model to the experimental data using optimization algorithms, due to the number of values in the lookup tables. This challenge is addressed using a layered approach to break the parameter estimation problem into smaller tasks. The size of each estimation task is reduced to a small subset of data and parameter values, so that the optimizer can better focus on a specific problem. The layered approach was successful in fitting an equivalent circuit model a data set. Moreover the model has been validated with different currents profiles such as RW and WLTP, which simulate the behaviour on road: urban, suburban roads and highway.

Furthermore, the model would be the starting point for building state of charge and health estimators of a battery by means of an Unscented Kalman filter (UKF). These estimators are essential for the correct management of the battery system during its operation. In fact, depending on the operating conditions, the battery could give or absorb certain quantities of energy according to certain power profiles.

This thesis work was developed at the LIM (mechatronics laboratory) at Politecnico di Torino.

Acknowledgements

"to my parents, friends, professors and those close"

Leonardo

Table of Contents

List of Tables	IX
List of Figures	X
Acronyms	XIV
1 Introduction	1
1.1 Overview	1
1.2 Organization of the thesis	3
1.3 Problem Statement	4
2 Lithium-ion Batteries: main characteristics and equivalent circuit modelling methods	5
2.1 Battery terminology and function	5
2.1.1 Preliminaries: cells and batteries	5
2.1.2 Voltage	6
2.1.3 Capacity and Charge/Discharge rate	7
2.1.4 Energy and power	7
2.1.5 Series and parallel connections	8
2.1.6 State of Charge and State of Health	8
2.1.7 How cells work	10
2.2 Battery models: state of the art	12
2.2.1 Internal resistance model	13
2.2.2 RC model	13
2.2.3 Thevenin model	14
2.2.4 Partnership for New Generation of Vehicle model	14
2.2.5 Dual Polarization model	16

2.3	Physical behaviour of a Li-ion battery model's component	18
2.3.1	Non Linear OCV characteristics	18
2.3.2	State of charge dependence	19
2.3.3	Internal resistance	21
2.3.4	Diffusion Voltages	23
2.4	Proposed model	25
3	Parameters characterization	28
3.1	Laboratory instrumentation	28
3.1.1	Test bench	28
3.1.2	Battery's technical specification	31
3.2	Test Procedure	34
3.2.1	Static capacity test	34
3.2.2	Constant Power Discharge and Charge Tests	34
3.2.3	Hybrid Pulse Power Characterization Test	35
3.2.4	Peak power test	37
3.2.5	WLTP	40
3.2.6	RW	40
3.3	Parameters characterization	42
3.3.1	Primal electrical parameters characterization	42
3.3.2	Electrical parameters characterization	43
3.3.3	Experimental data collected: Pulse discharge test	46
3.3.4	Choice of a 2nd order equivalent circuit model	47
3.3.5	Parameters estimation problem	49
3.3.6	Optimization problem formulation	51
3.3.7	Thermal model and its parameters estimation	52
3.3.8	Final parameter estimation	55
3.3.9	Model verification	62
4	Complete model and SOC estimation by means of UKF	65
4.1	UKF	66
4.1.1	What is an Unscented Kalman Filter?	66
4.1.2	UKF for SOC estimation	68
4.1.3	SOC estimator validation	72
4.1.4	SOH estimation	75

5 Conclusions and future development	77
Bibliography	80

List of Tables

2.1	Nominal voltage and energy specifications for different cell's chemistries	11
3.1	Battery technical specifications	31
3.2	HPPC test procedure	35
3.3	Thermal parameters	56

List of Figures

1.1	Sector responsible for emissions	2
2.1	Schematic symbols for a cell and a battery	6
2.2	Cell $LiFePO_4$	6
2.3	Battery pack $LiFePO_4$	6
2.4	Series	9
2.5	Parallel	9
2.6	Li-ion cell	11
2.7	R_{int} equivalent circuit	13
2.8	RC equivalent circuit	14
2.9	Thevenin equivalent circuit	15
2.10	PNGV model	15
2.11	Dual Polarization model	17
2.12	Battery with a constant output voltage	19
2.13	OCV(SOC)	21
2.14	Battery simplified model with OCV depending on SOC	21
2.15	Battery model, with SOC-dependent voltage and equivalent series resistance R_0	22
2.16	Polarization evident when a battery is subjected to a discharge pulse followed by a rest	23
2.17	Circuit that now models diffusion voltages	25
2.18	SOC and temperature dependent second-order RC equivalent circuit model.	26
3.1	Test bench	30
3.2	Software	30
3.3	Battery's chart and curves	33

3.4	Temperature measurement points	33
3.5	HPPC current profile vs time	36
3.6	HPPC complete procedure	37
3.7	USABC Energy Storage system Performance Targets for 48V Mild Hybrid Electric vehicles	38
3.8	Peak power test: current profile vs time	39
3.9	Peak power test complete procedure	39
3.10	WLTP cycle	40
3.11	Random walk cycle	41
3.12	Measuring Parameters values from a pulse response	43
3.13	parameters estimation flow chart	44
3.14	Discharge/Charge Pulse Test for electrical parameters characterization	45
3.15	Discharge Pulse Test on <i>LiFePO₄</i> 48V Battery	46
3.16	Fitting curves with different orders of ECM	47
3.17	Fitting curves to determine number of RC branches	47
3.18	experimental Data vs model exponential function	48
3.19	2RC equivalent circuit model	48
3.20	Equivalent circuit model for <i>LiFePO₄</i> battery with two parallel R-C branches	49
3.21	Parameter estimation procedure using simulink design optimization	50
3.22	Pulse test results	51
3.23	parameters values vs State of Charge	51
3.24	Thermal model developed in Simscape	54
3.25	Current and Voltage profile for thermal parameters estimation	55
3.26	Temperature measured vs simulated	56
3.27	Final parameter estimation with simulink design optimization	57
3.28	Open circuit voltage lookup table	57
3.29	Internal resistance lookup table	58
3.30	R_1 resistance lookup table	58
3.31	R_1 capacitance lookup table	59
3.32	R_2 resistance lookup table	59
3.33	C_2 capacitance lookup table	60
3.34	Voltage model output vs experimental data	63
3.35	Temperature model output vs data	63
3.36	Voltage's error	63
3.37	Temperature's error	63

3.38	Model tested on a WLTP profile	63
3.39	Model tested on a RW profile	64
4.1	SOC estimation scheme	68
4.2	Observer	68
4.3	State transition function and measurement function	69
4.4	Complete model developed in Simulink	71
4.5	UKF parameters set up	72
4.6	Pulse test current and voltage profile	73
4.7	Pulse test real SOC vs UKF estimate	73
4.8	WLTP current and voltage profile	74
4.9	WLTP real SOC vs UKF estimate	74
4.10	SOH estimation simulink scheme	76

Acronyms

EV

electric vehicle

GHG

Green house gasses

MHEV

mild hybrid electric vehicle

ICE

Internal Combustion Engine

SOC

State of Charge

SOH

State of Health

OCV

Open Circuit Voltage

ECM

Equivalent Circuit Model

RW

Random Walk

WLTP

Worldwide Harmonised Light Vehicle Test Procedure

HPPC

Hybrid Pulse Power Characterization Test

PNGV

Partnership for New Generation of Vehicle

DP

Dual Polarization

UKF

Unscented Kalman Filter

Chapter 1

Introduction

This chapter provides an introduction to the research conducted; including an overview on transports emissions problems and HEV, an organization of the thesis, and the problem statement.

1.1 Overview

Hazardous emissions and greenhouse gases (GHGs) are inevitable consequences of burning fossil fuels for energy. GHG emissions are the primary cause of rapid climate change, such as global warming and polar ice melting.

CO₂, NO_x, CO, and methane are the most common GHGs.

Figure ?? shows GHG emissions from various usage sectors, with transportation accounting for nearly 27%. The worldwide development and expansion of numerous urban areas have resulted in a significant increase in the number of vehicles on the road.

This high percentage of transportation GHG is, of course, due to the vehicle's internal combustion engine (ICE). As a result, decarbonization of transportation will eliminate the transportation sector's CO₂ emissions. This has motivated modern efforts to replace ICE-powered vehicles with alternative, sustainable, and clean power motors. Electrifying transportation is one promising approach to addressing the aforementioned health and environmental issues [1]. As a result, electric vehicles (EVs) have been viewed as a replacement for ICE vehicles. The EV has the potential for zero vehicle emissions, lower lifetime costs, and the use of

renewable energy. However, current EV technology is associated with issues such as limited range, high initial cost, and longer recharge time when compared to ICE vehicles. In many metropolitan areas and developing countries, the limited range of EVs may not be an issue. However, even in these suitable areas, the current lack of required fast-charging stations poses a barrier to entry.

Hybrid EVs are one option for overcoming the disadvantages of EVs (HEVs). HEV technology can be developed to address the shortcomings of both ICE vehicles and EVs. The HEV combines the advantages of the ICE and a battery-powered electric motor (EM) for transportation. When compared to ICE or EVs, these benefits include low emissions, high reliability, high fuel efficiency, and long range.[2]

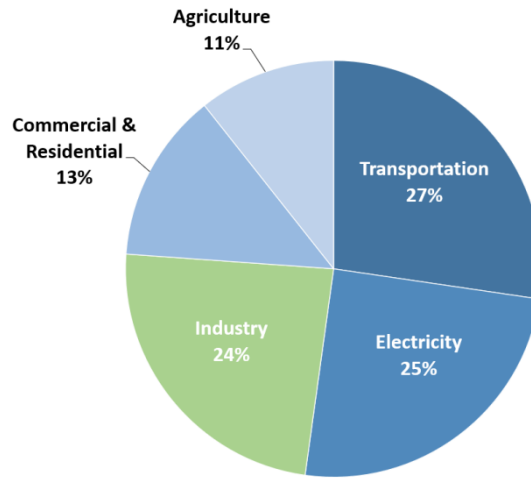


Figure 1.1: Sector responsible for emissions

In particular, the introduction of 48-Volt (48V) mild hybrid electric vehicles (MHEVs) has stimulated development of 48V battery systems capable of providing enhanced driving performance, higher energy density battery packs, and the improved life cycle durability required by consumers and necessary for full-useful-life compliance with emissions standards. Much of this activity has involved the development of advanced lithium chemistries and in some cases development of variations of deep-cycle lead-acid chemistries such as *LiFePO₄* formulation. Mild hybrid vehicles with 48V systems have appeared, few years ago, in the European light-duty vehicle market due to high fuel prices and stringent new European CO₂ car emissions standards.[3]

Within MHEV applications, an analysis of the battery pack performance, state-of-charge (SOC) optimization, is of importance since the overall efficiency of the vehicle is closely tied to the efficiency of the battery pack and the energy flows through the hybrid drive system. Mild hybrid vehicles employing 48V systems are expected to achieve significant growth in most major automotive markets in the near future. A 48V architecture brings a number of significant technical benefits to the vehicle and the battery itself will be much smaller, lighter and lower cost than high voltage alternatives.

1.2 Organization of the thesis

This thesis presents a combination of analytical and experimental research used to propose advancements in battery modeling, state of charge, and state of health estimation. The thesis is organized as follows:

- The second chapter provides a literature review on Lithium-ion batteries, first laying the foundations of how this works and introducing their main characteristics, then focusing on the state of art of different types of battery equivalent circuit models and explaining how battery's behaviour can be modeled.
- The third chapter proposes a state of charge parameterization strategy for identifying the parameters of a second order equivalent circuit model for the battery. Initially, the instrumentation used has been described (test bench and battery) with the related test procedure: Pulse test, Hybrid Pulse Power Characterization Test (HPPC), Random Walk (RW), Worldwide Harmonised Light Vehicle Test Procedure (WLTP). Furthermore, a parameter estimation problem is presented: the goal is to find the best estimate parameters in order to fit the data with the smallest possible error between the real data and the model, by means of the Simulink design optimization toolbox. Finally, a verification of the model is proposed through a WLTP driving cycle.
- The fourth chapter focuses on the SOC and SOH estimation through the use of an Unscented Kalman Filter and a Kalman Filter respectively. Moreover a complete analysis and testing of the model is proposed.

- The fifth chapter is about conclusions and future development of this thesis work.

1.3 Problem Statement

The four main focuses are:

1. *Modeling*: deriving mathematical expressions that describe how battery works. After several stages of development, the final models will include coupled sets of discrete-time ordinary difference equations that are functions of unknown but measurable or identifiable parameter values. The input to the models is the battery current; the output are the battery voltage and the battery internal states as well.
2. *Simulation*: using computer tools to predict how a battery will respond to an input stimulus. The equations of the battery model are used to predict voltage and possibly internal battery states. Will be presented simulations involving different current profile and will be given tips to implement the battery models in Matlab and Simulink enviroment.
3. *Identification*: determining the values of model parameters, using data obtained via laboratory tests, in order to let the model simulated predictions to match measured performance as closely as possible.
4. *Validation*: once the parameters of the model are identified, the model is tested with other types of input in order to verify if it works as expected.

Chapter 2

Lithium-ion Batteries: main characteristics and equivalent circuit modelling methods

2.1 Battery terminology and function

2.1.1 Preliminaries: cells and batteries

The National Electrical Code [4], defines a cell as “The basic electrochemical unit, characterized by an anode (i.e., negative electrode) and a cathode (i.e., positive electrode), used to receive, store, and deliver electrical energy.” Batteries are made of groups of cell; IEEE standard 446 [5] defines a battery as “Two or more cells electrically connected for producing electric energy.”

These cells can be electrically connected to each other both in series and in parallel to achieve the desired characteristics in terms of voltage, maximum current and capacity.

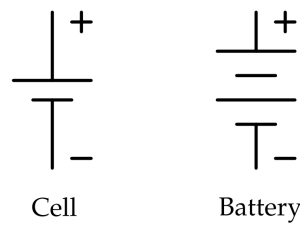


Figure 2.1: Schematic symbols for a cell and a battery



Figure 2.2: Cell $LiFePO_4$



Figure 2.3: Battery pack $LiFePO_4$

2.1.2 Voltage

Cell or battery voltage depends on a number of factors.

The manufacturer-specified *nominal voltage* is the value assigned to a cell or battery of a given voltage class for the purpose of convenient designation. The *operating voltage* of the cell or battery may vary above or below this value. Typically the voltage values of the individual cells range from 1.2V for Nickel-based chemistry cells to over 4V for Lithium-based cells but, usually, most Lithium-based cells have nominal voltages over 3V.

2.1.3 Capacity and Charge/Discharge rate

Cells store and deliver electrical charge to power a load circuit. The cell *nominal charge capacity* specifies the quantity of charge, in Ampere-hours (Ah) or milliAmpere-hours (mAh), that a cell is rated to hold. Note that the SI unit for charge is the coulomb (C) and that 1 Ah = 3600 C.

The cell's nominal energy (see below) is a different quantity. Both definitions of capacity have merit and can be computed from one another. However, as our focus in this thesis is on creating models that relate a battery's input current (i.e., rate of change of charge) to its internal state and output voltage, *charge capacity* turns out to be the more relevant concept. Unless otherwise mentioned, the term capacity will refer to charge capacity and not to energy capacity.

Related to the cell's charge capacity, the *C rate* is a relative measure of battery current. It is the constant-current charge or discharge rate that the cell can sustain for 1 hour. It is simply the nominal Ampere hour rating of the cell multiplied by $1h^{-1}$.

For example, a fully charged 25 Ah cell should be able to deliver 25A (i.e “1C” rate) for 1 h or 2.5 A (i.e “C/10” rate) for about 10 h before the cell is completely discharged. If the cell is discharged at a 10C rate, it will be completely discharged in about 6 minutes.

The capacity can be expressed by the equation 2.1:

$$Q = I\Delta t \quad (2.1)$$

Where Q is the capacity and its unit of measurement is the coulomb (C), I is the current (Ampere), Δt is the time (s). Note that the relationship between C rate and discharge time is not strictly linear, primarily because of the internal resistance of the battery cell and incomplete utilization of the active materials when the cell is exercised at high rates. In fact, a cell discharged at a 10C rate will reach a minimum operational voltage before 6 minutes has elapsed, but a cell discharged at a C/10 rate may be operated somewhat more than 10 h before reaching the minimum voltage.

2.1.4 Energy and power

A cell stores energy in electrochemical form, which can be later released to produce energy or power. The cell *nominal energy capacity* is the quantity of electrical

energy in Watt hours (Wh) or kiloWatt hours (kWh) that the cell is rated to hold and is computed as the cell's nominal voltage multiplied by its nominal charge capacity. For example, a 2V, 10Ah lead-acid cell has an energy storage capacity of roughly 20 Wh.

It is important to note that energy and power are different quantities for a particular rate of discharge.

Power power is the amount of energy transferred or converted per unit time. Power is measured in watts (W) or kilowatts (kW). The maximum power that a cell can deliver is limited by the cell's internal resistance and is not an easy value to quantify. Power is usually regulated by enforcing minimum and maximum limits on cell terminal voltage.

2.1.5 Series and parallel connections

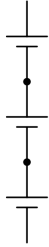
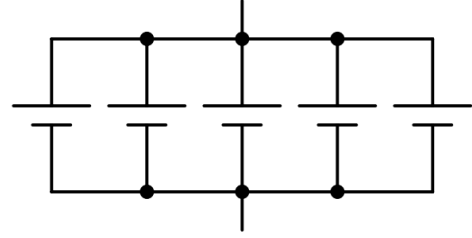
When cells are connected in *series*, the battery voltage is the sum of the individual cell voltages, by Kirchhoff's voltage law $\sum_{k=1}^N V_k = 0$. However, by Kirchhoff's current law $\sum_{k=1}^N I_k = 0$, the charge capacity of the series connected battery is the same as the charge capacity of an individual cell since the same current passes through all of the cells.

As an example, consider the battery in Fig 2.4, which is constructed from three 2 V, 20-Ah cells connected in series. The battery voltage will be 6 V, the battery charge capacity will be 20 Ah, and the battery energy capacity will be 120 Wh. When cells are connected in *parallel*, the battery voltage is equal to the cells' voltage, by Kirchhoff's voltage law. However, by Kirchhoff's current law, the charge capacity is the sum of the cells' charge capacities since the battery current is the sum of all the cell currents. For example, consider the battery in Fig 2.5, which is constructed from five 2V, 20-Ah cells connected in parallel. The battery will have a voltage of 2V, a charge capacity of 100 Ah, and energy capacity of 200 Wh.

2.1.6 State of Charge and State of Health

To define *the state of charge* (SoC), consider a completely discharged battery. Where $I(\tau)$ is the charging current, the charge delivered to the battery is $\int_{t_0}^t I(\tau)d\tau$. With $Q_0 = \int_{t_0}^\infty I(\tau)d\tau$ the total charge the battery can hold.

The state of charge (SoC) of the battery is simply given by:


Figure 2.4: Series

Figure 2.5: Parallel

$$SOC(t) = \frac{\int_{t_0}^t I(\tau)d\tau}{Q_0} 100 \quad (2.2)$$

Typically, it is desired that the state of charge of the battery be kept within appropriate limits, for example $20\% < SOC(\%) < 95\%$. As a consequence, it is essential to be able to estimate the state of charge of the battery to maintain the state of charge within safe limits. Estimating the battery state of charge (SoC) is not an easy task because the SOC depends on many factors such as temperature, battery capacitance and internal resistance as we will see later on[6].

Before introducing the SOH, it's necessary to give a definition of **battery capacity fading**: capacity loss or capacity fading is a phenomenon observed in rechargeable battery usage where the amount of charge that a battery can deliver decreases with use, this phenomenon is also called *aging* of the battery [7]. The same applies to battery's power: the more the battery ages the less the power available is.

The SOH of a battery could be expressed as the ratio of maximum available capacity in the present condition to the nominal capacity of the battery in a fresh condition. This can be stated as follows:

$$SOH(\%) = \frac{Q_{present}}{Q_{fresh}} 100 \quad (2.3)$$

where, $Q_{Present}$ denotes present available capacity of the battery and Q_{Fresh} indicates the capacity of the battery in the fresh condition (at beginning of life). In general, if battery capacity goes below 80% of its original capacity then the battery is considered as non-usable. This is due to exponential degradation of the

battery capacity exhibited below 80% cut-off. There are numerous internal and external factors influencing the health of the Li-ion battery and its performance degradation over a period of time. Some of the internal factors include battery material, calendar ageing and increase in internal resistance. The external factors are operating temperature, uncertain driving condition, overcharging/discharging, high charge/discharge rate and improper charge/discharge cycling. Due to many unknown and unpredictable factors influencing the health of the battery, estimating battery SOH becomes quite challenging [8].

2.1.7 How cells work

Cells are built from a number of principal components. These include a negative electrode, a positive electrode, the electrolyte, and a separator. Certain types of cells also have current collectors that are distinct from the electrodes themselves. Figure 2.6 shows a schematic of a Lithium-ion cell, but the basic idea applies generally. The negative electrode in an electrochemical cell is often a pure metal, or an alloy, or even hydrogen. The positive electrode in an electrochemical cell is often a metallic oxide, sulfide, or oxygen.

During discharge, the negative electrode gives up electrons to the external circuit, a process by which the electrode is oxidized: oxidation of a species involves the loss of electrons or, equivalently, an increase in the oxidation state of the species (it becomes more positively charged). During charge, the negative electrode accepts electrons from the external circuit and is reduced: reduction of a species involves the gain of electrons or, equivalently, a decrease in its oxidation state (it becomes more negatively charged). Thus, the chemical processes that occur in an electrochemical cell are sometimes called reduction–oxidation or redox reactions.

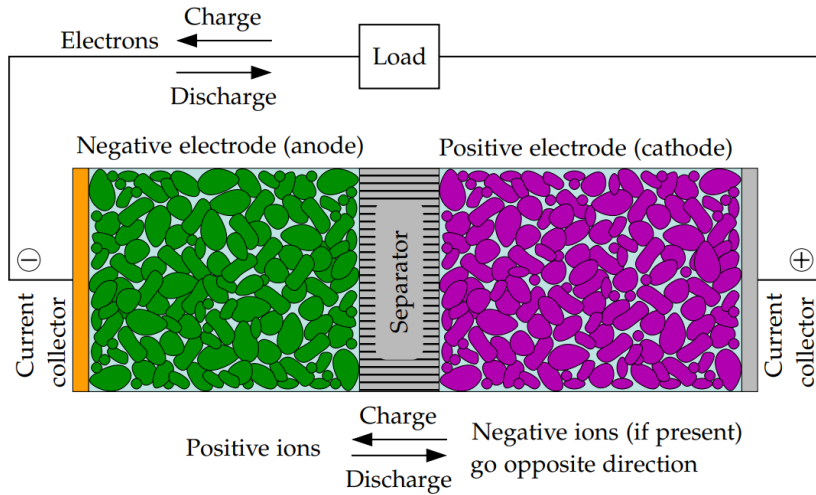


Figure 2.6: Li-ion cell

The table shows the main characteristics of the cells based on multiple technologies:

Characteristics of different cell types			
Cathode material	Nominal Voltage (V)	Energy Density (Wh/Kg)	Thermal stability
Cobalt Oxide	3.7	195	Poor
Nichel Cobalt Aluminium Oxide (NCA)	3.6	220	Fair
Nickel Cobalt Manganese Oxide (NCM)	3.6	205	Fair
Manganese Oxide (Spinel)	3.9	150	Good
Lithium Iron Phosphate (LFP)	3.2	130	Very Good

Table 2.1: Nominal voltage and energy specifications for different cell's chemistries

2.2 Battery models: state of the art

With the increased research in the fields of hybrid electric vehicle dynamic simulation as introduced in chapter 1, energy distribution and power control strategy, as well as the estimation of batteries' state of charge (SoC) and state of health (SoH) nowadays improving the accuracy of the charging and discharging model of power batteries, especially Lithium-ion batteries, is a significant objective.

Since the battery is a nonlinear system, the models usually used in mild hybrid electric vehicles (MHEVs) can be divided into three kinds: the simplified electrochemical model was proposed based on the electrochemical theory, and could fully describe the characteristics of the power battery by using mathematics to describe the inner action of the battery. For example, the Peukert equation can simply associate the power battery to an invariant linear system, however, it cannot handle its nonlinear characteristics and it can hardly simulate its dynamic performance. In order to overcome the drawbacks of the mathematical models, the neural network model was put forward, which took the weights of neurons into account instead of the state variables. The accuracy of this model could reach 3% under certain conditions. However, the accuracy and calculation burden of the model were influenced by the choices and quantity of input variables of the neural network. Also, a neural network trained by data can only be used within the original scope of that data. Based on the dynamic characteristics and working principles of the battery, the equivalent circuit model that are presented in this section are developed by using resistors, capacitors and voltage sources to form a circuit network. The circuit simulated the battery's internal resistance and dynamic effects such as terminal voltage relaxation. On a basis of the OCV estimate, SoC could be inferred via a lookup table, but this will be the argument of the next chapter. The equivalent circuit model has been widely used in various types of modeling and simulation for battery management systems. Evidently high dynamic simulation with high accuracy is one of the key technologies. [9]

In MHEV studies, various equivalent circuit models such as the R_{int} model, the RC model, the *Thevenin* model, and the *PNGV* model are now widely used. An improved Thevenin circuit model named *DP* (for dual polarization) is proposed to refine the polarization characteristics of a battery.

2.2.1 Internal resistance model

The internal resistance (R_{int}) model, as shown in Figure 2.7 and Equation 2.4, implements an ideal voltage source U_{OC} to define the battery open-circuit voltage. Both resistance R_0 (which is R_{int}) and open-circuit voltage U_{OC} are functions of SoC, SoH and temperature. I_L is load current with a positive value at discharging and a negative value at charging, U_L is the terminal voltage.

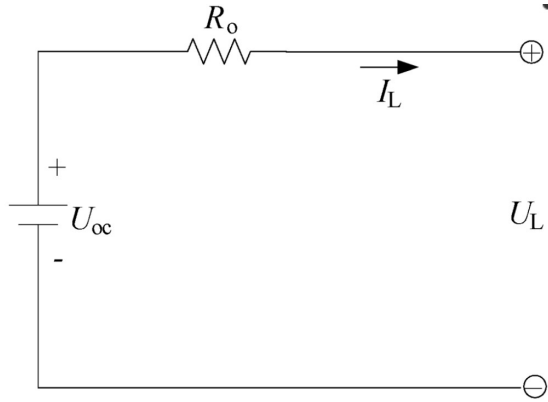


Figure 2.7: R_{int} equivalent circuit

$$U_L = U_{OC} - I_L R_o \quad (2.4)$$

2.2.2 RC model

The RC model, as shown in Figure 2.8, it consists of two capacitors (C_c, C_b) and three resistors (R_t, R_e, R_c). The capacitor C_c , which has a small capacitance and mostly represents the surface effects of a battery, is named surface capacitor. The capacitor C_b , which has a very large capacitance and represents the ample capability of a battery to store energy chemically, is named bulk capacitor. SoC can be determined by the voltage across the bulk capacitor. Resistors R_t, R_e, R_c are named terminal resistor, end resistor and capacitor resistor, respectively. U_b and U_c are the voltages across C_b and C_c , respectively. The electrical behaviour of

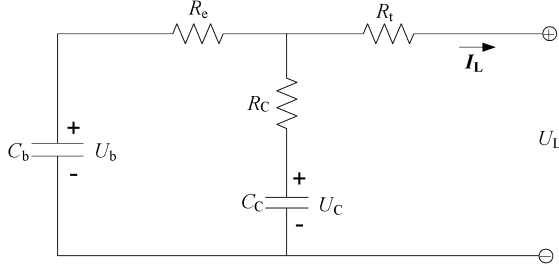


Figure 2.8: RC equivalent circuit

the circuit can be expressed by Equations 2.5 and 2.6.

$$\begin{pmatrix} \dot{U}_b \\ \dot{U}_c \end{pmatrix} = \begin{pmatrix} \frac{-1}{C_b(R_e+R_c)} & \frac{1}{C_b(R_e+R_c)} \\ \frac{1}{C_c(R_e+R_c)} & \frac{-1}{C_c(R_e+R_c)} \end{pmatrix} \begin{pmatrix} U_b \\ U_c \end{pmatrix} + \begin{pmatrix} \frac{-R_e}{C_b(R_e+R_c)} \\ \frac{-R_e}{C_c(R_e+R_c)} \end{pmatrix} (I_L) \quad (2.5)$$

$$(U_L) = \left(\frac{R_c}{R_e+R_c} \frac{R_e}{R_e+R_c} \right) \begin{pmatrix} U_b \\ U_c \end{pmatrix} + \left(-R_t - \frac{R_e R_c}{R_e+R_c} \right) (I_L) \quad (2.6)$$

2.2.3 Thevenin model

The Thevenin model connects a parallel RC network in series based on the R_{int} model, describing the dynamic characteristics of the battery. As shown in Figure 2.9, it is mainly composed of three parts including open-circuit voltage U_{oc} , internal resistances and equivalent capacitances. The internal resistances include the ohmic resistance R_0 and the polarization resistance R_{Th} . The equivalent capacitance C_{Th} is used to describe the transient response during charging and discharging. U_{Th} is the voltages across C_{Th} . I_{Th} is the outflow current of C_{Th} . The electrical behavior of the Thevenin model can be expressed by Equation 2.7 .

$$\begin{cases} \dot{U}_{Th} = -\frac{U_{Th}}{R_{Th}C_{Th}} + \frac{I_L}{C_{Th}} \\ U_L = U_{Th} - U_{OC} - I_L R_o \end{cases} \quad (2.7)$$

2.2.4 Partnership for New Generation of Vehicle model

The PNGV (Partnership for New Generation of Vehicle) model as shown in Figure 2.10 can be obtained by adding a capacitor $\frac{1}{U_{OC}}$ in series based on the Thevenin model to describe the changing of open circuit voltage generated in the time accumulation of load current. U_d and U_{PN} are the voltages across $\frac{1}{U_{OC}}$ and

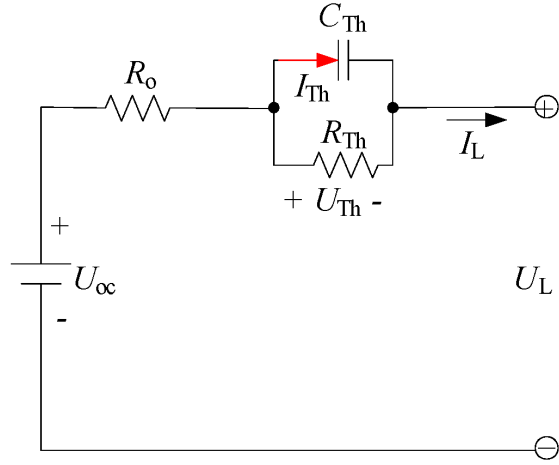


Figure 2.9: Thevenin equivalent circuit

C_{PN} respectively. I_{PN} is the outflow current of C_{PN} .

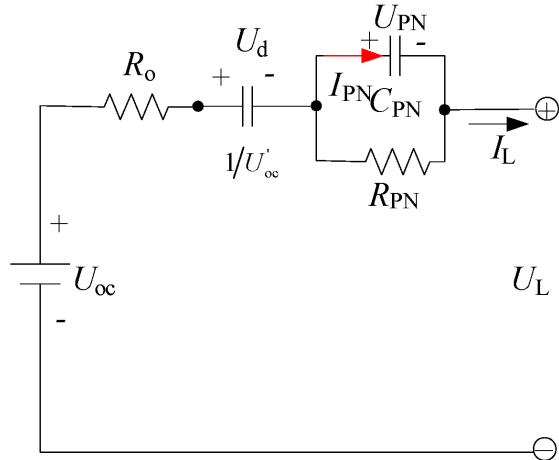


Figure 2.10: PNGV model

The electrical behavior of the PNGV model can be expressed by Equation 2.8:

$$\begin{cases} \dot{U}_d = U_{OC}I_L\dot{U}_{PN} = \frac{U_{PN}}{R_{PN}C_{PN}} + \frac{I_L}{C_{PN}} \\ U_L = U_{OC} - U_{PN} - U_d - I_L R_o \end{cases} \quad (2.8)$$

2.2.5 Dual Polarization model

Based on the test analysis of the characteristics of a lithium-ion power battery, an obvious polarization can be observed. The polarization characteristic could be simulated by the Thevenin model to some extent, however, the difference between concentration polarization and electrochemical polarization leads to an inaccurate simulation in the moments at the end of charge or discharge. An improved circuit model is presented in Figure 5, which is defined as Dual Polarization (DP) model, to refine the description of polarization characteristics and simulate the concentration polarization and the electrochemical polarization separately. The DP model is composed of five parts:

1. Open-circuit voltage U_{OC} ;
2. Internal resistances such as the ohmic resistance R_0 and the polarization resistances, which include R_{pa} to represent the effective resistance characterizing electrochemical polarization and R_{pc} to represent the effective resistance characterizing concentration polarization;
3. the effective capacitances like C_{pa} and C_{pc} , which are used to characterize the transient response during transfer of power to/from the battery and to describe the electrochemical polarization and the concentration polarization separately.
4. U_{pa} and U_{pc} are the voltages across C_{pa} and C_{pc} respectively.
5. I_{pa} and I_{pc} are the outflow currents of C_{pa} and C_{pc} respectively.

The electrical behavior of the circuit can be expressed by Equation 2.13:

$$\begin{cases} \dot{U}_{pa} = -\frac{U_{pa}}{R_{pa}C_{pa}} + \frac{I_L}{C_{pa}} \\ \dot{U}_{pc} = \frac{U_{pc}}{R_{pc}C_{pc}} + \frac{I_L}{C_{pc}} \\ U_L = U_{OC} - U_{pa} - U_{pc}I_L R_o \end{cases} \quad (2.9)$$

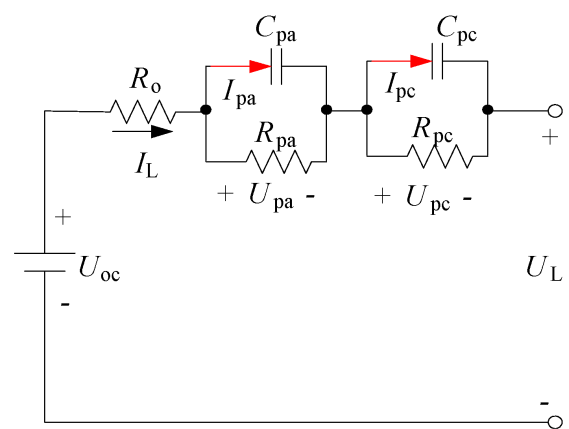


Figure 2.11: Dual Polarization model

2.3 Physical behaviour of a Li-ion battery model's component

Based on what has been introduced, the first step to create a battery model is to determine the final application in order to select the type that best suits the modeling needs. The applications examined in this study are those that provide energy and power to electric motor of a mild hybrid electric vehicle. The dynamics of interest therefore range from a few seconds to several hours. The model can be used as a foundation for developing SOC and SOH estimators. In fact, using the measured current and temperature data and running the model in simulated mode, it would be possible to analyze and understand the behavior of the storage system during operation. As a result, the battery pack , whose data are given by the manufacturer's datasheet in table 3.1, has no purpose to characterize the parameter of an equivalent circuit model of the battery, it only describes the operating range conditions and it's main specifications (voltage, current, temperature) at which the battery can work safely. Therefore, the circuit models are chosen because they provide the voltage and current information required to simulate the behavior of the battery pack.

Before defining the modalities on which the circuit model will be built, as shown in 2.11, the following assumptions must be made:

First and foremost, it is necessary to depict, the peculiar characteristics that a battery has at its terminals in order to determine which measurable factors can influence its behavior. Moreover, identifying the peculiar aspects that a battery has at its terminals, during charge/discharge process, is useful in establishing how the model will be built and the meaning of the various circuit elements that compose in, and their dependence on SoC and temperature.

2.3.1 Non Linear OCV characteristics

Let's start by explaining the most fundamental observed behavior of a battery: the voltage at its terminals. If a voltmeter across the terminals of a battery is placed, it will register some value. So, the first model we build represents the battery simply as an *ideal voltage source*. The schematic for this model is drawn in Fig. 2.12. In the model, battery terminal voltage $v(t)$ is not a function of load current $i(t)$, nor

is it a function of past battery usage. In fact, voltage is constant. This is a pretty poor model of a battery because terminal voltage of a real battery is dependent on load current, recent usage, and other factors as mentioned in [10].

However, this model provides a starting point for the battery development. Battery pack supplies a voltage to a load. And, when the battery is unloaded and in complete equilibrium (a condition that is termed open circuit), the voltage of the cell is fairly predictable. Hence, the voltage source in the model is labeled “OCV”. Will be shown that an ideal voltage source will remain a component of our final equivalent-circuit model.

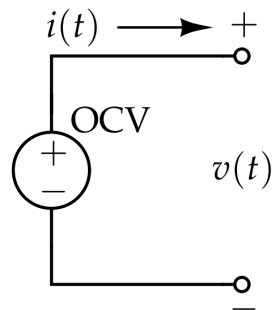


Figure 2.12: Battery with a constant output voltage

2.3.2 State of charge dependence

The first improvement to do is a result of recognizing that the voltage of a fully charged battery is generally higher than the voltage of a discharged battery. This is not, in fact, always the case, since the terminal voltage of the battery also depends on dynamic factors relating to how the battery has been used in the recent past. We can state, however, that the equilibrium unloaded rest voltage or open-circuit voltage of a fully charged battery is higher than that of a discharged battery. So, we can improve our model by including a relationship between the open-circuit voltage and the state of charge (SOC) . As said in 2.1.6, if the battery is at an intermediate state between being fully charged and fully discharged, its state of charge is somewhere between 0 % and 100 %. From now on, SOC will be denoted by the symbol z . To quantify state of charge, it's important to know how much charge a cell holds when it is fully charged versus how much charge remains when it

is fully discharged. So, we define the total charge capacity or more simply the total capacity of a cell to be the total amount of charge removed when discharging a cell from $z = 100\%$ to $z = 0\%$. (This is different from the cell's total energy capacity, as is discussed in section 2.1.3) Total capacity is usually measured in ampere-hours (Ah), and is denoted by the symbol Q . The value of total capacity is a parameter of the battery model. Total capacity is not a function of temperature or current, although the total capacity of a cell does tend to decrease very gradually as the ages due to undesired parasitic chemical side reactions and structural breakdown of the cell's electrode materials (as anticipated in 2.1.6). We can model changes to state of charge using an ordinary differential equation as:

$$\dot{z}(t) = -\frac{\eta(t)i(t)}{Q} \quad (2.10)$$

The term $\eta(t)$ is the *Coulombic efficiency* or charge efficiency of the battery. Creating an accurate model of Coulombic efficiency is a very challenging task, as its value depends on state of charge, charging rate, temperature, and the internal electrochemical state of the battery. However, due to the high Coulombic efficiencies of lithium-ion batteries, assuming that η is always equal to unity often gives reasonable overall model fidelity. It is possible to integrate the instantaneous relationship of 2.10 to obtain an aggregate equation for a change in SOC over some time interval. Given known state of charge at initial time $t_0 < t$, and known current between times t_0 and t , we get:

$$z(t) = z_0(t) - \frac{1}{Q} \int_{t_0}^t \eta(\tau)i(\tau)d\tau \quad (2.11)$$

In this equation, we use τ as a placeholder for the time variable inside the integral so that we do not confuse the dummy variable of integration (which should disappear from the final result when the integral is performed) with the upper limit of integration (which should be retained in the final result). Many times, we are more interested in a discrete-time model than a continuous-time model. Discrete-time models assume that the cell inputs and outputs are measured or sampled at a regular rate with period Δt seconds and frequency $\frac{1}{\Delta t}$ hertz. Such models are ready to be used inside inexpensive microcontrollers directly for battery management systems. To convert Eq. 2.11 to discrete time, let $t_0 = k\Delta t$ and $t = (k + 1)\Delta t$. Then, if we assume that the cell's input current is constant over the sampling interval Δt , we define:

$$z[k+1] = z[k] - \frac{\Delta t}{Q} \eta[k] i[k] \quad (2.12)$$

Having a mathematical model for state of charge, we are now ready to revise our circuit model. We first recognize that a battery's open circuit voltage is a function of its state of charge. Some examples taken from literature [11] are drawn in Figure 2.13. There is some temperature dependence to this relationship these curves are drawn for room temperature (25°C). Also, while these curves are drawn as functions of the battery's state of charge, it is also common to see them expressed in terms of the cell's depth of discharge (DOD): $DOD = 1 - z(t)$. The improved battery model, including open-circuit-voltage dependence on the cell's state of charge is depicted in figure 2.14. The ideal voltage source is replaced by a controlled voltage source having value equal to $OCV(z(t))$. If temperature dependence is required, we instead use $OCV(z(t), T(t))$, where $T(t)$ is the cell's internal temperature at time t . The OCV values for a battery are determined empirically at numerous SOC points via laboratory procedures described in the next chapter. These values can be stored in a lookup table, such that the OCV function is evaluated via interpolation between table entries.

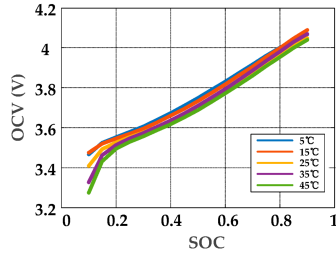


Figure 2.13: OCV(SOC)

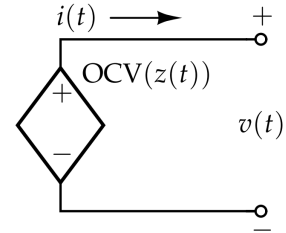


Figure 2.14: Battery simplified model with OCV depending on SOC

2.3.3 Internal resistance

Up until this point, the model that we have developed is essentially static. It describes the rest behavior of the battery. Now, we begin to add dynamic features to the model to describe what happens when the battery is subjected to a time-varying input current $i(t)$. The first observation that we would like the model to describe is that the battery's terminal voltage drops below the open-circuit voltage when the

battery is subjected to a load, and the terminal voltage rises above the open-circuit voltage when the battery is being charged. This phenomenon can be explained in part by placing a resistance in series with the controlled voltage source. The revised model is drawn in figure 2.15:

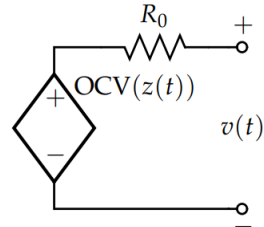


Figure 2.15: Battery model, with SOC-dependent voltage and equivalent series resistance R_0

The added circuit component represents the so-called *equivalent series resistance* (ESR) of the battery. In the revised model, the state of charge equation remains unchanged. However, we add a second equation to the model to describe how to compute the terminal voltage:

$$\begin{cases} z[k+1] = z[k] - \frac{\Delta t}{Q} \eta[k] i[k] \\ v[k] = OCV(z[k]) - i[k] R_0 \end{cases} \quad (2.13)$$

Note that the presence of this series resistance in the model also implies that power is dissipated by the cell internal resistance as heat (Joule effect), and therefore the energy efficiency of the cell is not perfect. The power dissipated by the equivalent series resistance can be expressed as:

$$P_{joule} = i^2(t) R_0$$

Finally, we note that the battery's resistance is often a function of the battery's state of charge and is always a function of the battery's internal temperature. The fidelity of the model's predictions will be enhanced if these dependencies are taken into account in R_0 . This model of a battery is sufficient for many simple electronic-circuit designs. However, it is not yet adequate for applications in large-scale battery packs, such as for electric-drive vehicles or mild hybrid electric vehicles. There are other dynamic features that must be considered as the transient between

working and rest condition of the battery.

2.3.4 Diffusion Voltages

Polarization refers to any departure of the battery's terminal voltage away from open-circuit voltage due to a passage of current through the cells. In the equivalent-circuit model that we have developed so far, we have modeled instantaneous polarization via the $i(t)R_0$ term. Real batteries have more complex behavior, where the voltage polarization slowly develops over time as current is demanded from the battery and then slowly decays over time when the battery is allowed to rest. Figure 2.16 illustrates this behavior:

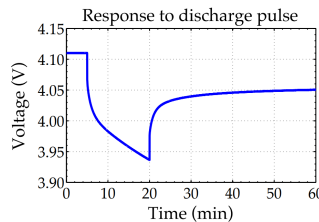


Figure 2.16: Polarization evident when a battery is subjected to a discharge pulse followed by a rest

The voltage plotted in 2.16 corresponds to the following scenario:

1. the battery is at rest for the first 5 min, and the voltage is constant;
2. the battery is then subjected to a discharge current pulse of constant magnitude from $t = 5$ min until $t = 20$ min;
3. the load is removed, and the battery is allowed to rest for the remainder of the test.

The model developed so far explains the battery behavior during the initial rest. It also explains the immediate *voltage drop* when current is applied and the immediate *voltage recovery* when the current is removed. It is difficult to predict, without further analysis, whether the battery model accurately predicts the voltage during the discharge interval, since we know that state of charge is decreasing, and so too the open-circuit voltage is decreasing. But we know for certain that the third section of the test is not being well modeled. In this section, we see that voltage

is constantly changing, but we also know that the battery state of charge is not changing since the battery current is zero. There is something going on here that is not yet part of our model. If you have ever played with a flashlight, you are certain to have seen this phenomenon in action. What happens when your battery is just about empty? The light produced by the flashlight grows dimmer and dimmer and becomes indiscernible. But turn the flashlight off and wait a minute or two. Then turn the flashlight back on—the bulb is brighter again! Did the battery magically recharge? No, but its voltage recovered somewhat from the slow decay in polarization that we observed in Figure 2.16, and we are able to get (a little) more light from the flashlight with nearly empty batteries. We will find out later that this phenomenon is caused by slow diffusion processes of lithium in a lithium-ion cell, so we will refer to this slowly changing voltage as a *diffusion voltage*. Its effect can be approximated closely in a circuit using one or more parallel resistor–capacitor subcircuits. In figure 2.17, the combination of R_1 and C_1 perform this function. In the model, the state-of-charge equation remains the same as before, but the voltage equation changes to:

$$\begin{cases} z[k+1] = z[k] - \frac{\Delta t}{Q} \eta[k] i[k] \\ v[k] = OCV(z[k]) - i[k] R_0 - R_1 i_{R_1}[k] \end{cases} \quad (2.14)$$

or in continuous time:

$$\begin{cases} \dot{z}(t) = z(t) - \frac{\Delta t}{Q} \eta(t) i(t) \\ v(t) = OCV(z(t)) - i(t) R_0 - R_1 i_{R_1}(t) \end{cases} \quad (2.15)$$

Where the expression for the resistor current $i_{R_1}(t)$ by the Kirchoff current law is: $i(t) = i_{R_1}(t) + i_{C_1}(t)$, where $i_{C_1}(t)$ is the current that flows through C_1 . Further, we have that $i_{C_1}(t) = C_1 \dot{v}_{C_1}(t)$, which gives: $i_{R_1}(t) + C_1 \dot{v}_{C_1}(t) = i(t)$. Then, since $v_{C_1}(t) = R_1 i_{R_1}(t)$, we have:

$$\frac{di_{R_1}(t)}{dt} = -\frac{1}{R_1 C_1} i_{R_1}(t) + \frac{1}{R_1 C_1} i(t) \quad (2.16)$$

Summarizing to date, the continuous-time model that describes the circuit in Figure 2.17 is:

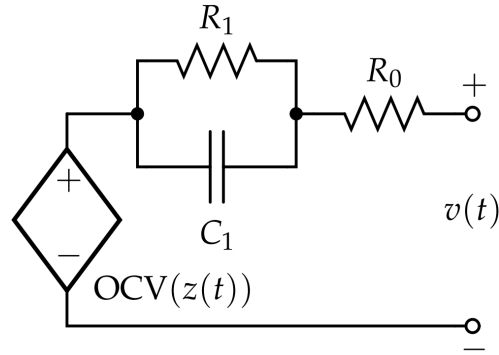


Figure 2.17: Circuit that now models diffusion voltages

$$\begin{cases} \dot{z}(t) = z(t) - \frac{\Delta t}{Q} \eta(t) i(t) \\ v(t) = OCV(z(t)) - i(t)R_0 - R_1 i_{R_1}(t) \\ \frac{di_{R_1}(t)}{dt} = -\frac{1}{R_1 C_1} i_{R_1}(t) + \frac{1}{R_1 C_1} i(t) \end{cases} \quad (2.17)$$

Finally, if we transform the equations in discrete time we have:

$$\begin{cases} z[k+1] = z[k] - \frac{\Delta t}{Q} \eta[k] i[k] \\ v[k] = OCV(z[k]) - i[k]R_0 - R_1 i_{R_1}[k] \\ i_{R_1}[k+1] = \exp(-\frac{\Delta t}{R_1 C_1}) i_{R_1}[k] + (1 - \exp(-\frac{\Delta t}{R_1 C_1})) i[k] \end{cases} \quad (2.18)$$

2.4 Proposed model

At different temperatures, the battery's characteristics change dramatically. Temperature variation factors should be considered in the battery modeling process to improve the battery model's temperature adaptability. The electrical characteristics of Lithium-ion batteries at various ambient temperatures are first discussed in this section. Then, taking into account the effects of ambient temperature variations, a temperature-dependent second-order RC (Dual Polarization) model is established. [12].

As said before in 2.3.2 the OCV is closely related to the battery SOC and the ambient temperature, and it is crucial for Lithium-ion battery modeling and SOC estimation. As shown in Figure 2.13, the OCV of the Lithium-ion battery gradually decreases as the ambient temperature rises. On the basis of the influence of ambient

temperature on Lithium-ion batteries just introduced, a temperature-dependent second-order RC equivalent circuit model is established in this section, taking into account both model accuracy and model complexity. This model is composed of three modules:

1. the OCV module
2. the internal resistance module R_0 .
3. the RC network module.

The structure of the proposed model is shown in figure 2.18, where V_t represents the battery terminal voltage, V_{OCV} indicates the OCV, V_1 and V_2 denote the voltages generated by the polarization phenomenon, I stands for the current (positive for charging and negative for discharging), T represents the ambient temperature, R_0 is the ohmic internal resistance, R_1 and R_2 are the polarization internal resistances, and C_1 and C_2 are the polarization capacitances. It must be pointed out that the effects of *SOC*, *temperature*, and *current direction* changes on the above parameters have been taken into account in the battery modeling, as we will explain in the next paragraph.

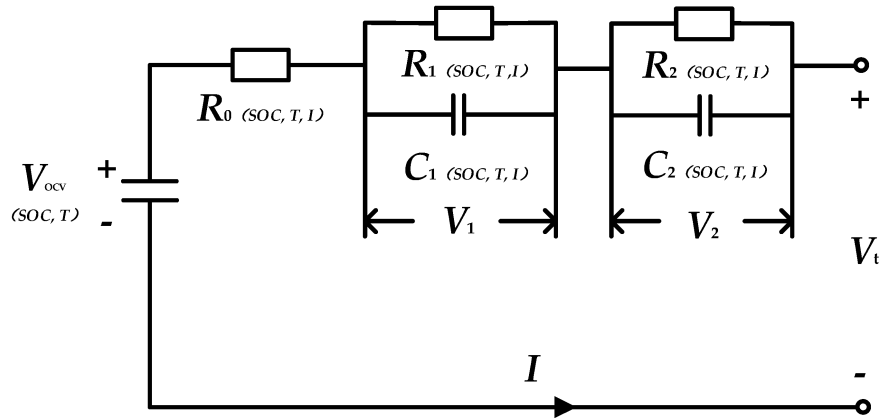


Figure 2.18: SOC and temperature dependent second-order RC equivalent circuit model.

According to Kirchhoff's laws of voltage and current, the polarization voltages V , V_1 and V_2 satisfy the following rules:

$$\begin{cases} \dot{z}(t) = z(t) - \frac{\Delta t}{Q}\eta(t)I(t) \\ V = V_{OCV} + V_1 + V_2 + R_0I \\ \dot{V}_1 = -\frac{V_1}{R_1C_1} + \frac{I}{C_1} \\ \dot{V}_2 = -\frac{V_2}{R_2C_2} + \frac{I}{C_2} \end{cases} \quad (2.19)$$

Transforming the equations from continuos to discrete time we have:

$$\begin{cases} z[k+1] = z[k] - \frac{\Delta t}{Q}\eta[k]I[k] \\ V[k] = V_{OCV} - i[k]R_0 - R_1i_{R_1}[k] - R_2i_{R_2}[k] \\ V_1[k+1] = \exp\left(\frac{-\Delta t}{R_1C_1}\right)V_1[k] + R_1I[k]\left(1 - \exp\left(\frac{-\Delta t}{R_1C_1}\right)\right) \\ V_2[k+1] = \exp\left(\frac{-\Delta t}{R_2C_2}\right)V_2[k] + R_2I[k]\left(1 - \exp\left(\frac{-\Delta t}{R_2C_2}\right)\right) \end{cases} \quad (2.20)$$

Equations 2.19 and 2.20 constitute the mathematical representation of the proposed temperature-dependent second-order RC model for lithium-ion batteries. These equations describe the dynamic characteristics of lithium-ion batteries at different temperatures, in a simple mathematical form with limited number of parameters. Some parameters in this proposed battery model are not known a priori and need to be determined for model implementation. The parameters to be identified are R_1 , R_2 , C_1 , C_2 , R_0 , and V_{OCV} . In the following chapter, we shall explain in detail how these unknown parameters can be identified.

Chapter 3

Parameters characterization

The following section is intended to illustrate the technical specifications of the battery and the instrumentation used in the course of the experimental activity. The various test procedures followed for the determination of the different battery parameters, necessary for the subsequent construction of an equivalent model, are then illustrated.

The activity involves the use of a cycler, consisting in an electronic load and a power supply. The procedure is divided into several parts. The first consists of the general aspects concerning the charge and discharge of the battery. The second concerns the determination, again by means of the simulink design optimization toolbox, of the electrical parameters of the circuit model previously introduced.

3.1 Laboratory instrumentation

3.1.1 Test bench

In figure 3.1 is presented the instrumentation used to perform the tests on our battery. Here follows a detailed list of the instruments used for testing the battery

- The *IT5100 battery tester* is a series of battery internal resistance testers with high precision, high resolution and high speed. IT5100 adopts AC 4-terminal sensing, that means the tester can test internal resistance and voltage simultaneously with high precision. Resistance resolution is down to $0.1 \mu\Omega$, voltage resolution is $10 \mu V$. Combined with external USB disk, IT5100 is available for long-term statistics calculation. Built-in comparator function,

IT5100 can automatically determine whether the battery parameters meet the standards and count pass rate, which is suitable for a variety of battery's test and pick. Built-in USB / LAN communication interface to support SCPI communication protocol. Single unit of IT5102 support 16 channels batteries measurement, master- slave connection up to maximum 17 sets and extension channels quantity up to 272, that greatly improves testing efficiency. Built-in LAN / RS232 communication interface, IT5100 series can be widely applied in cellphone lithium batteries, electric vehicle batteries and other batteries inspection and sorting.

- The *bi-directional programmable DC power supply of IT6000C series* (Cycler in figure 3.1) combines two functions in one: source and sink with energy regeneration. Based on these functions, IT6000C offers the functionality of two-quadrant operation. The regenerative capability enables the energy consumed to be fed back to the grid cleanly, saving costs from energy consumption and cooling, while not interfering with the grid. IT6000C series provides 5 voltage grades with a maximum output voltage of 2250V. It supports master-slave paralleling with averaging current distribution, maximum output power up to 1.152MW. Built-in waveform generator supports generating arbitrary waveforms, and import LIST files for waveforms via front panel USB port. IT6000C is the combination of high reliability, high efficient setting, safe and multiple measurement functions.
- *ITS5601 is ITECH multi-channel temperature logger* used for temperature monitoring. ITECH multi-channel temperature logger is available for monitoring temperature via 24 channels at a time. The specifications of the temperature logger are as follows: measurement range -200°C - 2000°C, measurement accuracy 0.5°C and resolution 0.01°C. The superior performance of temperature logger makes it possible for ITECH Test System to acquire temperature data effectively and accurately and for wide application of the system in testing of batteries of all kinds.
- *ITS5000 Test System software* (figure 3.2) is equipped with a user-friendly interface. The simple and compact edit interface allows you to execute complex test program without mastery of any programming language, making programming as easy as filling out documents.

Moreover ITS5000 Test System provides the users with an array of charge/discharge modes such as CC/CP/CR discharge mode and it can simulate constant voltage charge and constant current charge modes. Various end-of-discharge conditions contribute to improvement of testing safety and prevention of over-discharge and overcharge of battery. The “AND” + “OR” logical relation may be established among time, capacity and voltage end-of-discharge conditions to cater to more complex testing requirements.



Figure 3.1: Test bench

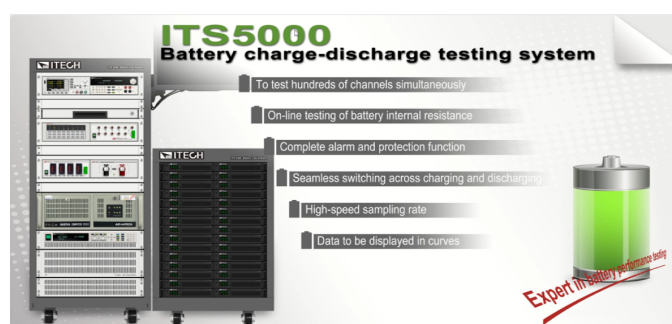


Figure 3.2: Software

3.1.2 Battery's technical specification

Here follows a table of technical specifications of the battery used to conduct laboratory tests:

Electrical specifications	
Nominal voltage	51.2 V
Nominal Capacity	25 Ah
Stored energy	1280 Wh
Internal resistance	< 50 mΩ
Cycles	> 3000 cycles (see chart)
Self discharge	< 3% per month
Energy efficiency	>98%
Standard Charge specifications	
Charge Voltage	57.6 ± 0.8 V
Charge mode	CC/CV : Constant Current / Constant Voltage
Continuous charge current	12.5 A
Maximum charge current	25 A
BMS charge cut-off voltage	59.2 V ± 0.4V
Standard Discharge specifications	
Continuous discharge current	50 A (2.56 kW)
Maximum discharge current	100 A (5.12kW)
BMS discharge cut-off voltage	40V
Environment specifications	
Charge temperature range	0°C to +50°C
Discharge temperature range	-20°C to +60°C
Storage temperature	0°C to +50°C with 60±25 % relative humidity
IP protection level	IP 66
Mechanical specifications	
Cell assembly	26650 - 16S8P
Casing material	ABS
Dimensions	L:260mm x P:168mm x H:212 mm
Weight	12.6 kg
Terminal	M8

Table 3.1: Battery technical specifications

Furthermore, the battery presents the following characteristics:

- High Service Life: 3000 cycles and more (see chart 3.3).
- Deep discharge allowed up to 100 %.
- Ultra safe Lithium Iron Phosphate chemistry (no thermal run-away, no fire or explosion risks).
- Embedded BMS (Battery Management System) : improve lifespan and secure the battery.
- Calendar life > 10 years.
- Excellent temperature robustness (-20 °C up to +60 °C).
- Flexible deployment : up to 10 packs in parallel and 2 in serial.
- Constant power during discharge (very low internal resistance).
- Very low Peukert's losses (energy efficiency >98 %).
- Very low self discharge (<3 % per month).
- No memory effect.
- About 50 % lighter and 40% smaller than equivalent Lead-AGM battery with same usable energy.
- Certification : CE, RoHS, UN 38.3, UL and CB.

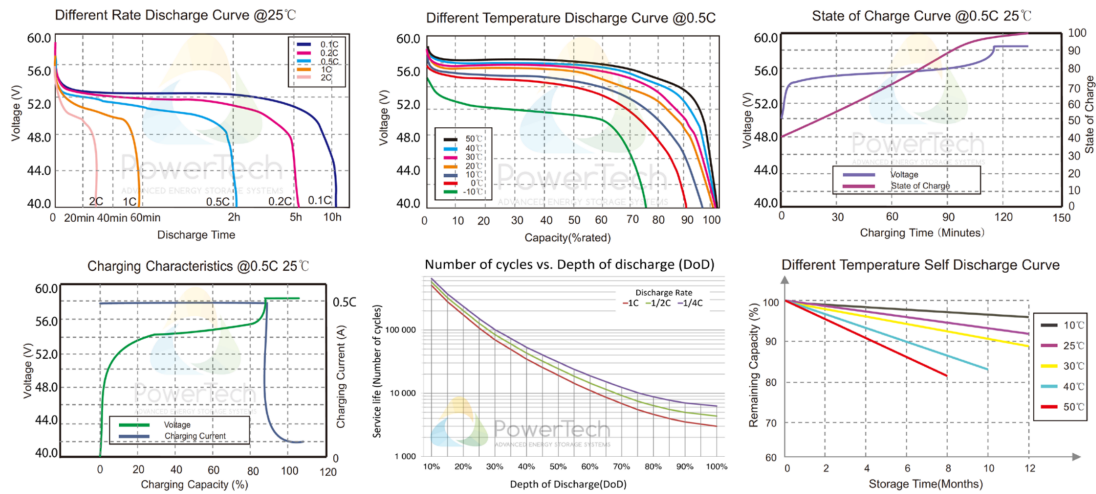


Figure 3.3: Battery's chart and curves

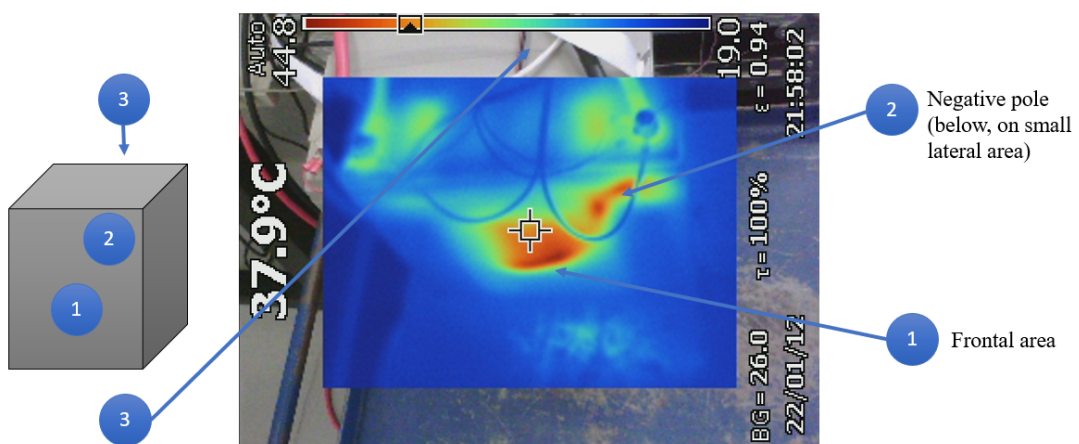


Figure 3.4: Temperature measurement points

3.2 Test Procedure

For the construction of the lithium-ion cell model, the following test procedure was defined, useful for determining the different parameters of interest. The section is divided into different parts, one of which concerns the general test aspects from literature, one concerning the basic tests, one for the determination of the model parameters, and one for the validation of the model, generally a WLTP. This procedure has been defined referring to valid for the analysis of a battery.

3.2.1 Static capacity test

The static capacity test is used to verify the manufacturer rated capacity, and it is performed as follows:

- Start: battery is fully charged ($V_{max100\%}$)
- Discharge: constant current 1C
- End: battery fully discharged (V_{min0})
- Then: default-rest at OCV (Open Circuit Voltage) is performed.

This test is to be performed until three consecutive discharge capacities are stable within $\pm 2\%$ up to a maximum of 10 discharges. This test can also be repeated using V_{maxop} as the fully charged condition to ensure stable operating capacity as well.

3.2.2 Constant Power Discharge and Charge Tests

This test measures device capacity in ampere-hours and energy in watt-hours at a constant power discharge rate. The constant power value will be a scaled power that is 5 times the Available Energy at the Beginning of Life (BOL).

This test is divided in the following phases:

- battery fully charged (V_{maxop})
- 1h rest (but it depends on the needs of the battery's chemistry)
- discharge down to voltage limit (V_{min0})
- 1h rest at open circuit voltage (OCV)

- Charge at constant power

This test can also be performed using the HPPC-Current rate between the top of the operating window and V_{min0} for comparison with the constant power discharge. The HPPC-Current is calculated using the formula below:

$$I_{HPPC} = \frac{P_{CPD}}{V_{nominal} * BSF}$$

Where: P_{CPD} is the Constant Power Discharge target (Wh), $V_{nominal}$ is average electrochemical voltage between V_{max100} and V_{min0} (i.e., total energy divided by capacity) and BSF is the battery scaling factor.

3.2.3 Hybrid Pulse Power Characterization Test

The Hybrid Pulse Power Characterization (HPPC) Test is intended to determine the 30-sec discharge-pulse and the 10-sec regen-pulse power capabilities at each 10% increment relative to the Beginning of Life (BOL) operating capacity for the HEV Targets (e.g., for a 25 Ah battery, power capabilities are assessed at 2.5 Ah increments between V_{maxop} and V_{min0}).

Time increment (s)	Cumulative time (s)	Relative Current
30	30	1
40	70	0
10	80	-0.75

Table 3.2: HPPC test procedure

- Full Discharge at 1C
- 1h rest
- Battery full recharged to V_{maxop}
- 1h rest
- HPPC profile
- Discharge to the next 10 % increment of the rated capacity at 1C

- rest 1h
- Repeat the phases from 5 to 7 till the 90 % of the rated capacity is removed (10 % SOC)
- Discharge to V_{min0} at 1C
- Final rest

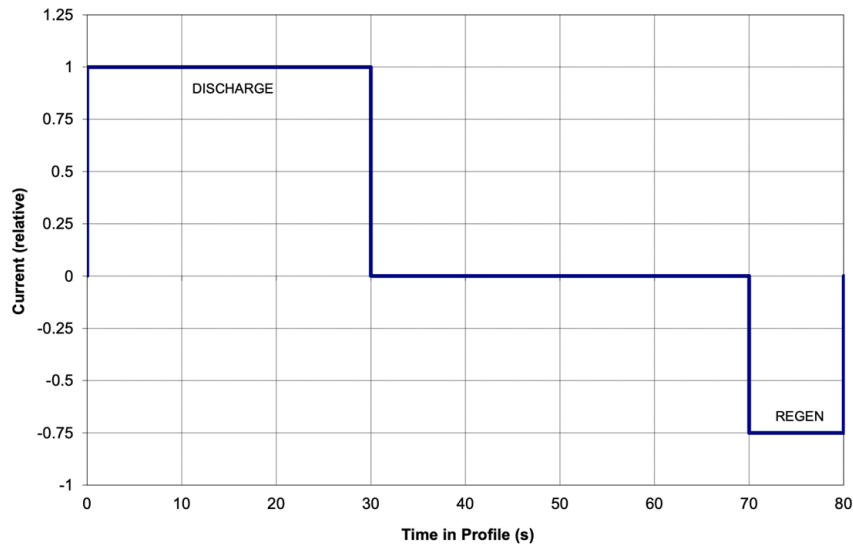


Figure 3.5: HPPC current profile vs time

Rest periods allow the battery to return to an electrochemical and thermal equilibrium condition. The primary purpose of the HPPC test is to periodically verify how the 1s Discharge Pulse, 10s Discharge Pulse, 5s Regen Pulse, and Available Energy for a given test article compare to the appropriate targets identified in Table 3.7. To achieve this purpose the data need to be captured during the HPPC test for successful comparison with the targets:

- Temperature of the test article during the HPPC test.
- Cumulative capacity (Ah) removed at the end of each 10 % increment based on rated capacity, defined at beginning of life and fixed throughout life testing.
- Cumulative capacity (Ah) removed at the end of each discharge pulse within the HPPC profile.

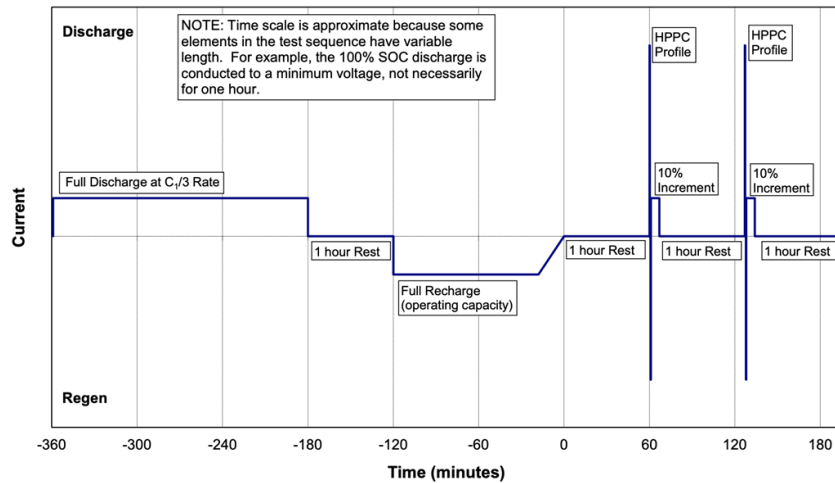


Figure 3.6: HPPC complete procedure

- Measured voltages at the start, at 1 s, at 10 s for the discharge pulse and at the start, at 5 s during the regen pulse with the HPPC profile.
- Measured currents at the start, at 1 s, at 10 s for the discharge pulse and at the start, at 5 s during the regen pulse with the HPPC profile.

From these data, the analysis methodology described here in can be used to determine the BSF-scaled values that are to be compared with targets in table.

To achieve this purpose the data need to be captured during the HPPC test for successful comparison with the targets:

- Temperature of the test article during the HPPC test. Cumulative capacity (Ah) removed at the end of each 10 % increment based on rated capacity, defined at beginning of life and fixed throughout life testing. Cumulative capacity (Ah) removed at the end of each discharge pulse within the HPPC profile.

3.2.4 Peak power test

The test consists of:

- Discharge at a given Base Current
- Periodic discharge pulses at a High test Current starting from Vmaxop.

End of Life Characteristics	Units	Target
Peak Pulse Discharge Power, 10s	kW	9
Peak Pulse Discharge Power (1s)	kW	11
Peak Regen Pulse Power (5s)	kW	11
Cold cranking power at -30 °C (three 4.5-s pulses, 10s rests between pulses at min SOC)	kW	6-kW for 0.5s followed by 4 kW for 4s
Accessory Load (2.5 min duration)	kW	5
Available Energy	Wh	313¹
CS 48V HEV Cycle Life	Cycles/MW h	75,000 /21.8
Calendar Life at 30°C	Years	15
Minimum round trip energy efficiency	%	95
Maximum allowable self-discharge rate	Wh/day	2
Maximum Operating Pulse Voltage	Vdc	52
Minimum Operating Pulse Voltage	Vdc	38
Minimum Voltage During Cold Crank	Vdc	26
Unassisted Operating Temperature Range (Power available to allow 5s charge and 1s discharge pulse) at min. and max. operating pulse SOC	°C	-30 to + 52
30 °C – 52 °C	kW	11
0 °C	kW	5.5
-10 °C	kW	3.3
-20 °C	kW	1.7
-30 °C	kW	1.1
Survival Temperature Range	°C	-46 to +66
Maximum System Weight	kg	≤8
Maximum System Volume	L	≤8
Maximum System Selling Price (@250k units/year)	\$	\$275

Figure 3.7: USABC Energy Storage system Performance Targets for 48V Mild Hybrid Electric vehicles

- No rest periods.

Objective: determine the 30-sec discharge-pulse power capabilities at each 10 % increment relative to the BOL operating capacity (as HPPC but with a different profile).

The Base Current is established based on the equation:

$$I_{baseCurrent} = \frac{[(12C_{operating}) - I_{HighTestCurrent}]}{35}$$

Where $C_{operating}$ is the device's operating capacity between V_{maxop} and V_{min0} .

The High test Current should be the maximum rated pulse current for the device (I_{max}).

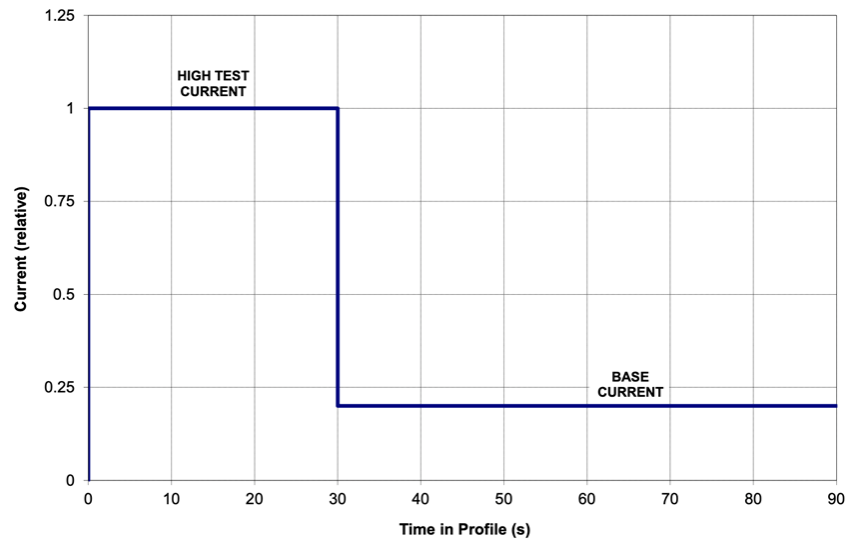


Figure 3.8: Peak power test: current profile vs time

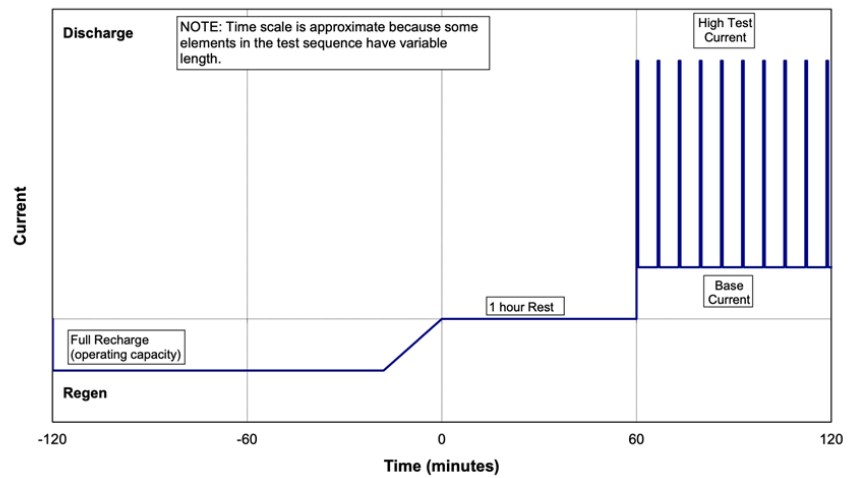


Figure 3.9: Peak power test complete procedure

3.2.5 WLTP

WLTP stands for *Worldwide Harmonised Light Vehicle Test Procedure* and is a global harmonized standard for determining the levels of pollutants, CO_2 emissions and fuel consumption of traditional and hybrid cars, as well as the range of fully electric vehicles. The procedure works over a longer test cycle and with more acceleration and braking events, higher speeds and shorter times spent at standstill, this means that there are short current peaks of different module with a frequency depending on the accelerating or braking events. Typically the events are grouped into average velocity bands, likewise those of the WLTP database (which is originally based on peak velocities between two stops), and these are divided in three road-types (urban, rural and motorway) as shown in figure 3.10, where are illustrated three different average speed: low, medium and high and their respective power values [13].

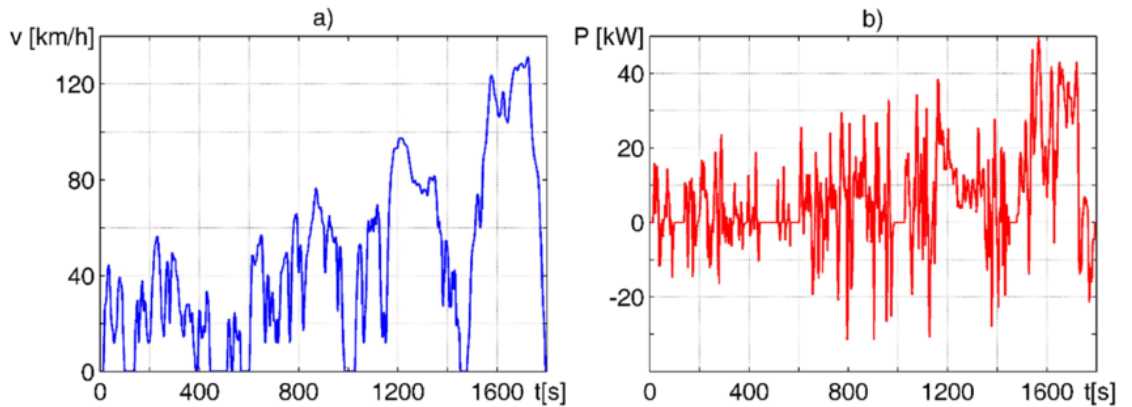


Figure 3.10: WLTP cycle

This type of profile will be used to verify the battery model in the next section.

3.2.6 RW

The Random Walk profile is a test that give as input a random current profile between 2 limits (50 A and -50A). A randomly selected charging or discharging current is applied to a battery for every five-minute which is specified as a step in the dataset. Negative currents are associated with discharging and positive currents indicate charging operation. For every five-minute duration a new current is chosen randomly and applied to the battery. To ensure battery safety operation, battery

voltage is charged to its maximum threshold voltage and discharged to its minimum threshold voltage. Whenever a battery runs beyond its voltage range during its step operation, then the current step operation stops and new step operation is initiated by choosing a new value from the current set. After every step, a small amount of delay of approximately 1 s is permitted to choose a new current value which is described as rest (random walk) in the dataset and repeated for every step. Even though the exact driving pattern of the MHEV is not imitated by the RW profile, it makes best attempt to capture the dynamic operating condition of the MHEV with the help of a random current set, and it has been used for aging the battery we tested.

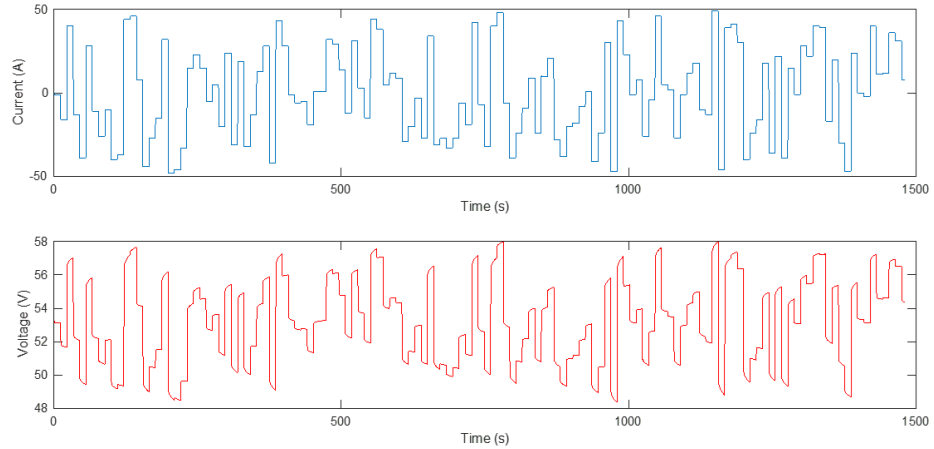


Figure 3.11: Random walk cycle

3.3 Parameters characterization

3.3.1 Primal electrical parameters characterization

We give a more general procedure later on, but at this point we can introduce a simple method that helps us understand how the parameters of the equations describe battery responses. In this section, we assume a model type of the sort developed to this point, having a double parallel resistor–capacitor subcircuit exactly as drawn in figure 2.18.

To identify the model parameters we subject the battery to a constant current discharge pulse and then we allow it to rest while recording the cell voltage response shown in Figure 3.12. At the instant when the discharge current pulse is removed, at time 300s, and considering eq. 2.20, the instantaneous change in voltage must be equal to the instantaneous change in current multiplied by the series resistance R_0 because the capacitor voltage cannot change instantly, and state of charge is not changing when current is zero. This gives us $\Delta V_0 = R_0 \Delta i$ (with signs computed such that R_0 is positive). We know the change in current $\Delta i = 25A$, because we controlled its value during the test, and we measure the change in voltage; therefore, we can compute the value $R_0 = |\frac{\Delta V_0}{\Delta i}|$. Then, we look at the steady-state change in voltage, which we can approximate by the value around time 600 seconds. The overall steady-state voltage change can be found from equation 2.20 to be $\Delta V_\infty = (R_0 + R_1 + R_2)\Delta i$, again with signs computed so that R_0 , R_1 and R_2 are both positive, knowing that the capacitor voltage will converge to zero in steady state. Since we know Δi (it's the same as when we were computing R_0), we measure this new value of ΔV , and as we have already computed R_0 , we can compute $R_1 + R_2 = |\frac{\Delta V_\infty}{\Delta i}| - R_0$. For the cell test conducted to gather the data plotted in figure 3.12, $\Delta i = 25A$, the change in voltage at time 300 seconds was $\Delta V = 2.12V$, and the change in voltage at time 600 seconds was $\Delta V = 0.375V$.

From these values, we compute $R_0 = 0.085\Omega$ and $R_1 + R_2 = 0.015\Omega$.

Finally, the pulse response converges to a value close to steady state in about 4 time constants of the R–C circuit, where the time constants of the exponential decay is $\tau_1 = R_1 C_1$ and $\tau_2 = R_2 C_2$. In our case, the time to convergence is about 600s - 300s = 300s. So, for this example, we might estimate $4\tau = 1200s$ where τ accounts the effects of both $R_1 C_1$ and $R_2 C_2$. Later on, a model based procedure developed in the matlab and simulink environment will be propose for a more accurate characterization of the parameters. This method is designed to give

rough estimates of the parameter, and the results obtained for each parameter (V_{OCV} , R_0 , R_1 , R_2 , C_1 , C_2) will be used as starting point for the estimation through an optimization algorithm. Fine-tuning can be done using the approach described in the next subsection.

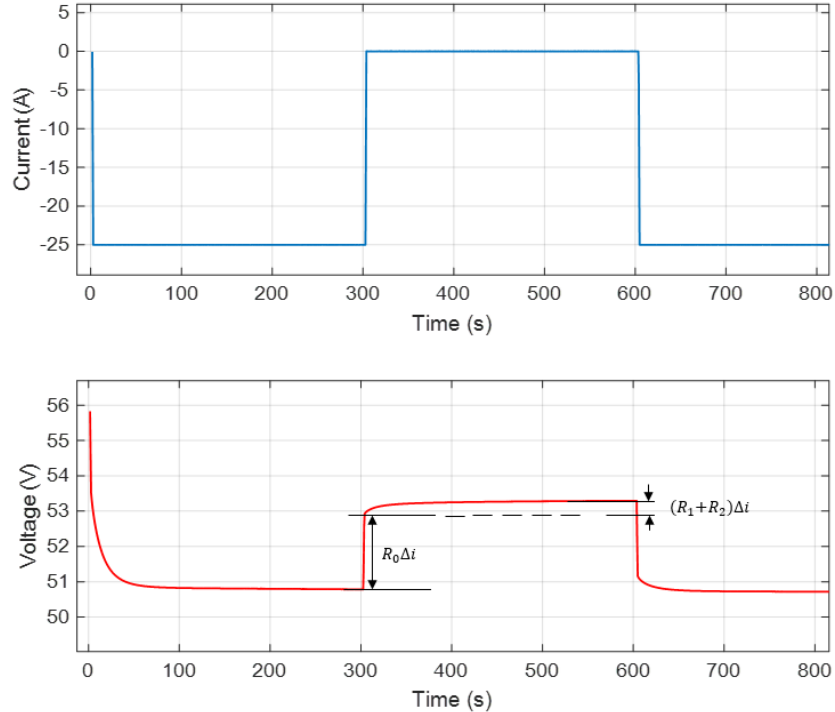


Figure 3.12: Measuring Parameters values from a pulse response

3.3.2 Electrical parameters characterization

The goal here is to parameterize the equivalent circuit values as function of environmental condition (temperature °C) and state of charge (SoC) based on measurement data. We will use an optimization technique in order to fit the model's output to experimental data. The method by which the parameters will be obtained is illustrated very simply in the flow chart in figure 3.13.

Charge curves as shown in figure 3.14, or mixed discharge/charge pulses sometimes referred to as highperformance pulse characterization (HPPC) data curves introduced in 3.2.3. Parameter estimation using this data involves repetitive computer simulation of the equivalent circuit model with the use of a *numerical*

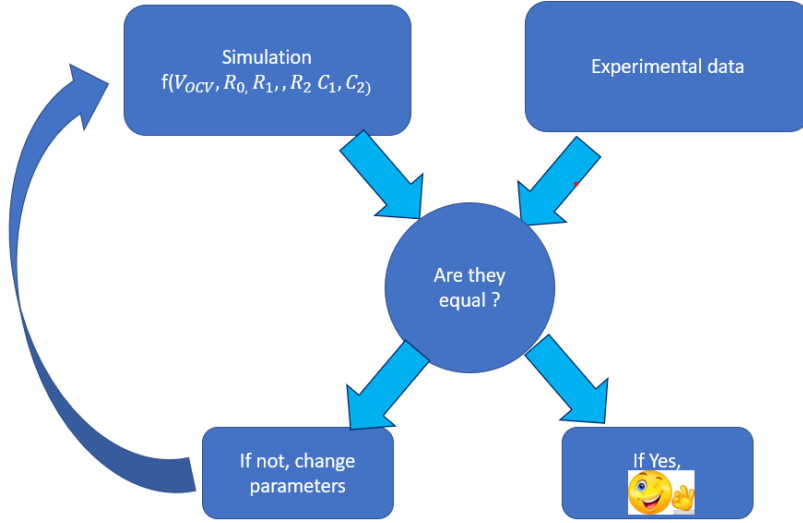


Figure 3.13: parameters estimation flow chart

optimization algorithm. The optimization adjusts parameters to minimize error between each experimental battery data set and the corresponding simulated results, given identical input signals [14]. Pulse curves help to provide a high-fidelity representation of battery performance, including the transient response, at multiple state-of-charge (SOC) and temperature values. To incorporate this high-fidelity representation into equivalent circuit model the operating conditions and states of the battery cell. *Lookup tables* are frequently used to provide this flexibility.

Previous work has shown lookup tables present unique challenges when using numerical optimization routines to determine the parameters for a specific battery. Fitting the entire set of lookup tables in a single estimation task worked well with a simpler model for lithium nickel manganese cobalt (NMC) cells, but it did not yield acceptable results for *LiFePO₄* cells. The *LiFePO₄* cells tested exhibited more complex transient dynamics including notable hysteresis. It was found that having too little flexibility in the model for *LiFePO₄* data caused the optimization routine to get stuck. In this case, the simulated result would not converge toward the measured cell data. To correct this problem, we added more flexibility by placing additional R-C branches in the equivalent circuit as mentioned in 2.4, but this also made the parameter estimation significantly more complex compared to a first-order equivalent circuit model. A common approach to solve a complex estimation is to break up the problem into multiple smaller tasks, before scaling

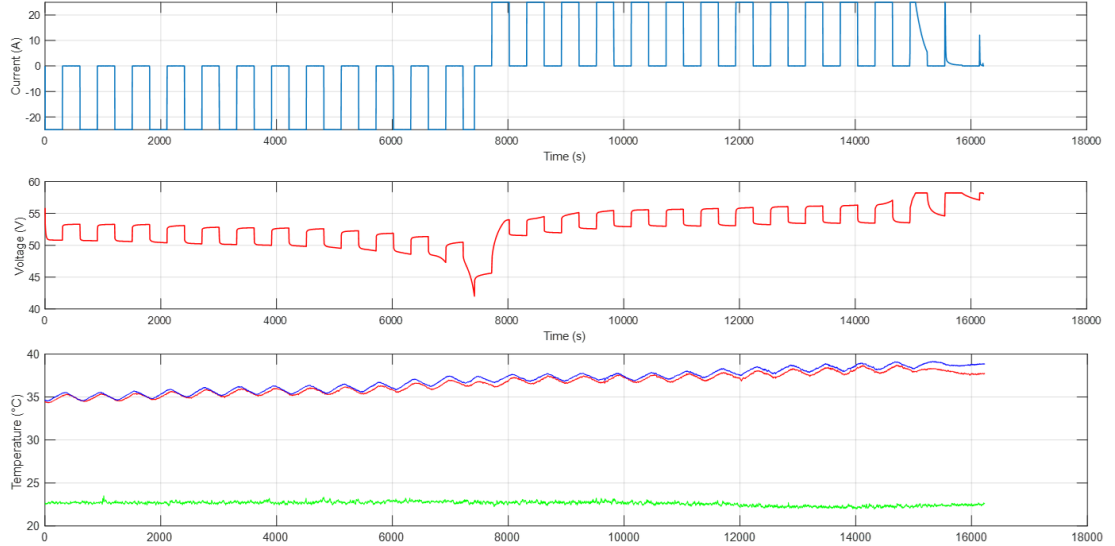


Figure 3.14: Discharge/Charge Pulse Test for electrical parameters characterization

up to a larger estimation problem, i.e. separate the discharge and the charge cycle. This way, each optimization problem is simpler, and will be more likely to converge on a desired solution. Independent variables that can be held relatively constant, such as temperature, can be easily split into separate estimation tasks. However, SOC changes dynamically during the test conditions. There is not a straightforward way to break up the pulse discharge curves to estimate parameters at each individual SOC breakpoint in the lookup tables. The proposed approach involves layering optimization tasks to estimate the parameters along the SOC breakpoints of a lookup table. The estimation tasks must be defined in a way that the data sufficiently exercises the “free” parameters that are being tuned during that task. However, the task must also have enough free parameters that the optimization routine can achieve a good fit to the measured data. Layering estimation tasks significantly increases the number of estimation steps that are needed. However, it reduces the complexity of each task by greatly reducing the number of free parameters in each task. In the sections that follow, we discuss:

- The experimental data we collected.
- The parameter estimation problem, and the proposed layered approach.
- How we implemented and automated the parameter estimation.

- The final results of the estimation process

3.3.3 Experimental data collected: Pulse discharge test

To populate the lookup tables, it was necessary to acquire data that exercise each of the parameters in those tables. Pulse type tests such as in Figure 3.15 provided necessary data about the performance of the battery cell at different points of SOC. The number of pulses taken and their width had an effect on the resolution of the data content, since each pulse provided content at specific SOC breakpoints. We chose a discharge test with uneven SOC breakpoints, as shown in Figure 3.15. The discharge test included pulses of 10% discharge amounts. The high and low SOC pulses were taken while discharging 10% of cell capacity. This way, we had more data at high and low SOC to better characterize those regions where performance may change dramatically. Figure shows just one example dataset. To fully parameterize the lookup tables, additional datasets would be needed to cover the desired operating range of the cell, including different temperatures and currents.

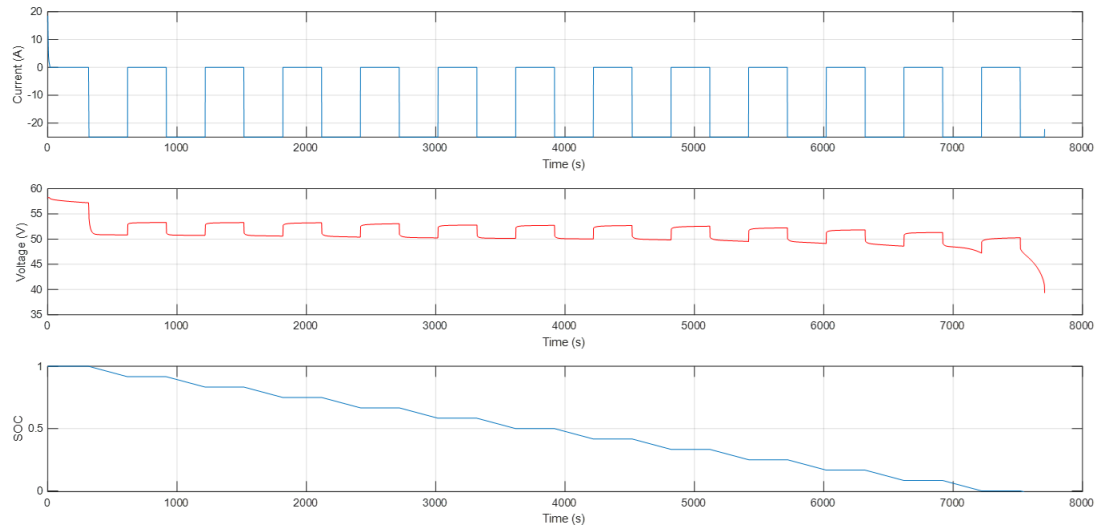


Figure 3.15: Discharge Pulse Test on $LiFePO_4$ 48V Battery

3.3.4 Choice of a 2nd order equivalent circuit model

In the analysis of the relaxation voltage, conducted in [15], the voltage's curve is generally based on the time constants, which is used to represent the recovery speed of the terminal voltage. Figure 3.16 shows a typical relaxation curve and the fitting curves with different orders of ECM. It can be seen from Figure 3.16 that fitting the relaxation voltage curve with a single RC link is inferior, and as the amount of RC link increases, that is, with more time constants, the fitting curve tends to be more accurate. In another research conducted by [14] is shown that having too little or too much flexibility in the model could cause the optimization to get stuck. In this case, the simulated result would not converge at all toward the measured battery voltage data. To determine the number of R-C branches to use, data are examined during the relaxation phase. When the pulse current was removed, the transient response was dictated by the R_0 and the R-C branches from the equivalent circuit from Figure 3.17. The first sample after the pulse is ignored, making the assumption that the instantaneous voltage change was described by the R_0 parameter. Then one or more exponential equations is fit to the data using Curve Fitting Toolbox. Regardless of the number of exponentials that are used in this example, they predominantly focused on the slow time constant.

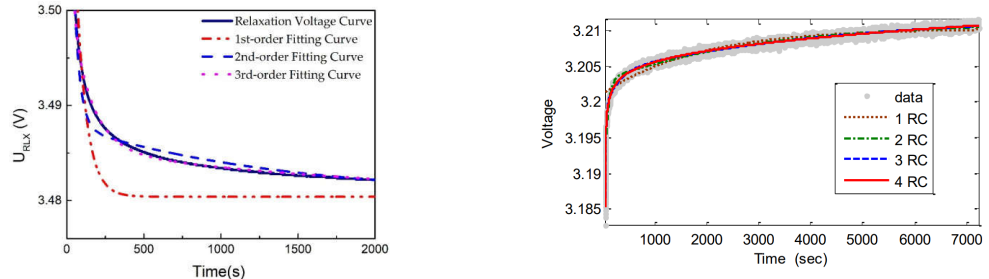


Figure 3.16: Fitting curves with different orders of ECM

Figure 3.17: Fitting curves to determine number of RC branches

For what concerns our battery, the data and the model output obtained for just one pulse relaxation phase at 50% SOC are represented in figure 3.18.

The exponential cost function used for curve fitting is:

$$F = R_1(1 - e^{\frac{-t}{\tau_1}})\Delta i + R_2(1 - e^{\frac{-t}{\tau_2}})\Delta i \quad (3.1)$$

Where R_1 and R_2 are the 2 resistors of the 2 RC branches, while τ_1 and τ_2 are

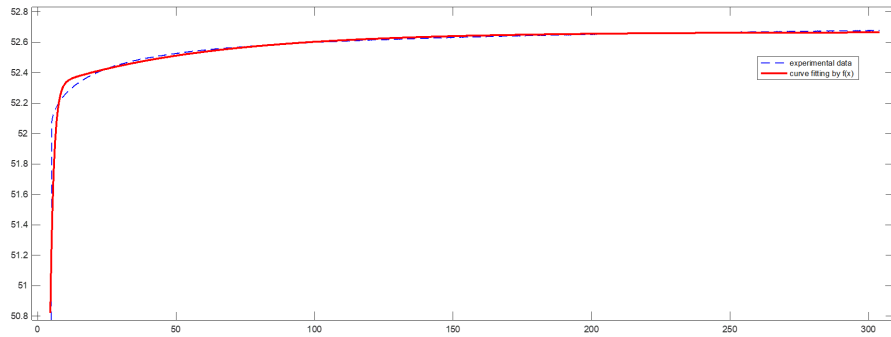


Figure 3.18: experimental Data vs model exponential function

the fast and the low time constant respectively, from which is possible to compute the values of the capacitance $C_1 = \tau_1/R_1$ and $C_2 = \tau_2/R_2$.

From this results, we determined that having just one exponential time constant terms did not produce a satisfactory match to the data. While the curve fit with four exponentials had the lowest residual error but high complexity, we chose a 2 time constants as a compromise between accuracy and computational cost. The equivalent circuit model with 2 R-C branches, and neglecting parasitic losses, is shown in figure 3.19

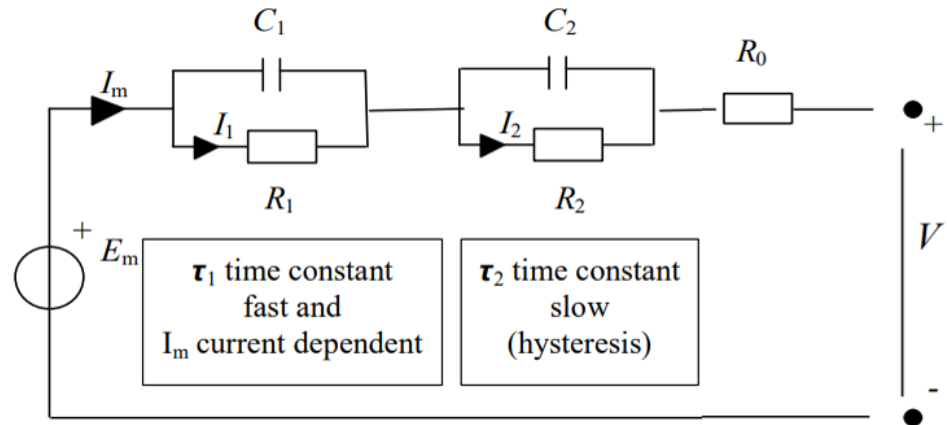


Figure 3.19: 2RC equivalent circuit model

The model based on the 2 R-C branches circuit shown in figure 3.19 has been developed in Simulink, in particular in the Simscape environment that allows to create custom circuit elements containing lookup tables. This model was needed to generate the simulation results to optimize the parameter values, and is shown in figure 3.20

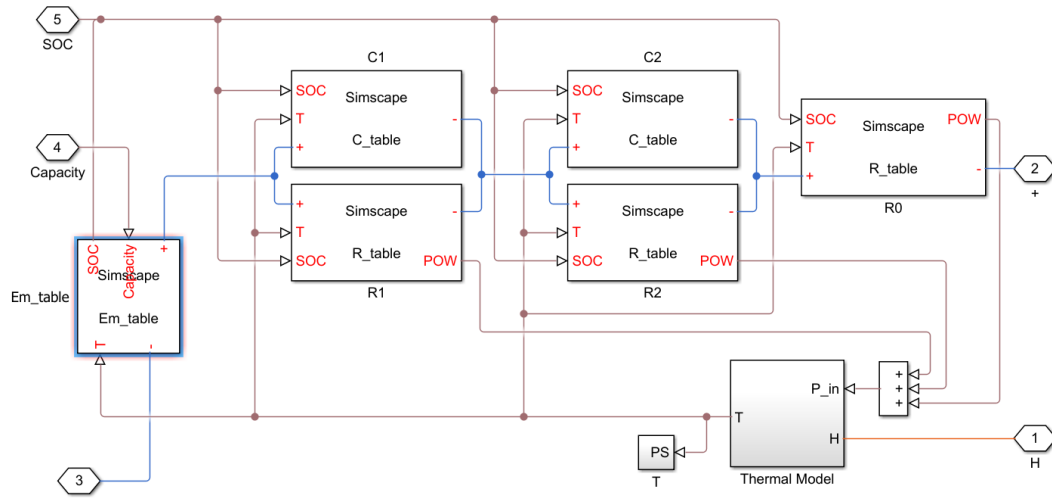


Figure 3.20: Equivalent circuit model for $LiFePO_4$ battery with two parallel R-C branches

3.3.5 Parameters estimation problem

The equivalent circuit with two R-C branches had six variable electrical circuit elements that are a function of the operating conditions. These circuit elements were represented by lookup tables. If considering multiple operating conditions, these tables would become quite large. In this thesis, we considered just 3 temperatures and one discharge current. However, additional independent operating conditions would simply require repeating the estimation process for each condition, and populating additional dimensions of the tables. Based on the data in Figure 3.15 containing 10 pulses, we calculated the corresponding 10 values of SOC that occurred before and after each pulse. We represented the values of each circuit element with lookup table versus the 10 points of SOC and the 3 of temperature. Because of the 2 R-C branches, the 10 number of SOC breakpoints and the 3

different temperatures ($25, 35, 45^{\circ}\text{C}$), given the data in Figure 3.15, we had 30 parameters for each lookup table, thus, a total of 180 electrical parameters to estimate, which are quite a lot parameters.

For this reasons, the problem has been divided in different steps.

If you have more than one RC branch in the model, then initial conditions (i.e initial guesses) for the parameters are very important. In fact, starting from good initial condition of the parameter makes a big difference in avoiding local minima and finding the best overall result. So we used an rough parameter estimation as mentioned in 3.3.1 technique to measure approximate values for the parameters before starting this estimation process by means of an optimization algorithm. Of course the analytical solution makes some assumptions that are only approximately true so it didn't give a perfect result.

Moreover, during the first estimation process with the use of Simulink optimization toolbox, the temperature has been neglected at this first step. In this way the lookup tables where composed only by 10 entries, each entry corresponding to a SOC value. Thus, in this step the total number of parameters to estimate was 60. The first estimation procedure is shown in figure 3.21

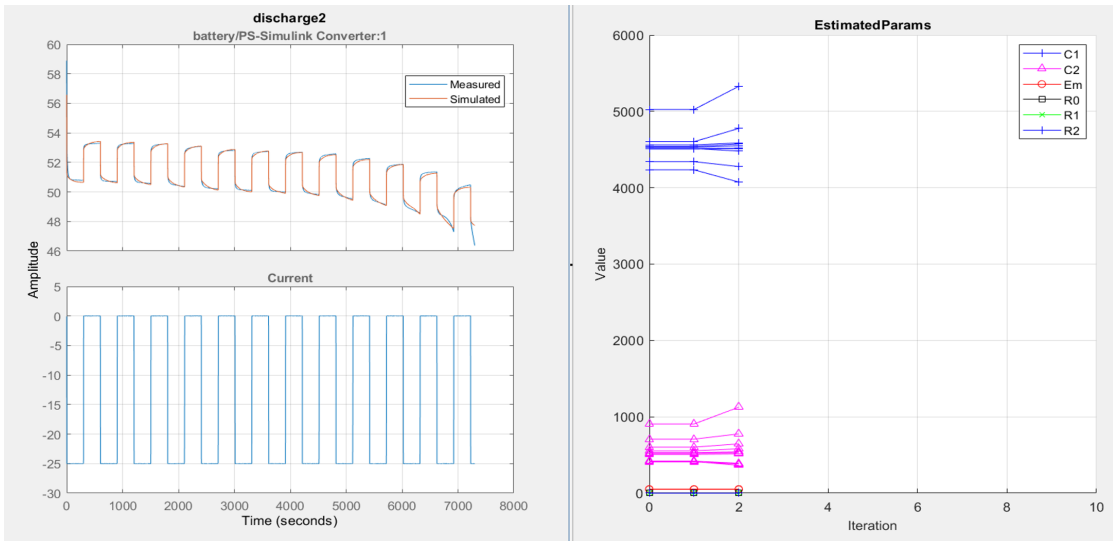


Figure 3.21: Parameter estimation procedure using simulink design optimization

The results of this estimation problem are represented in the plot in figure 3.22: And the parameters value obtained for this estimation are shown in figure 3.23. Before continuing with the characterization of the parameters I would like to

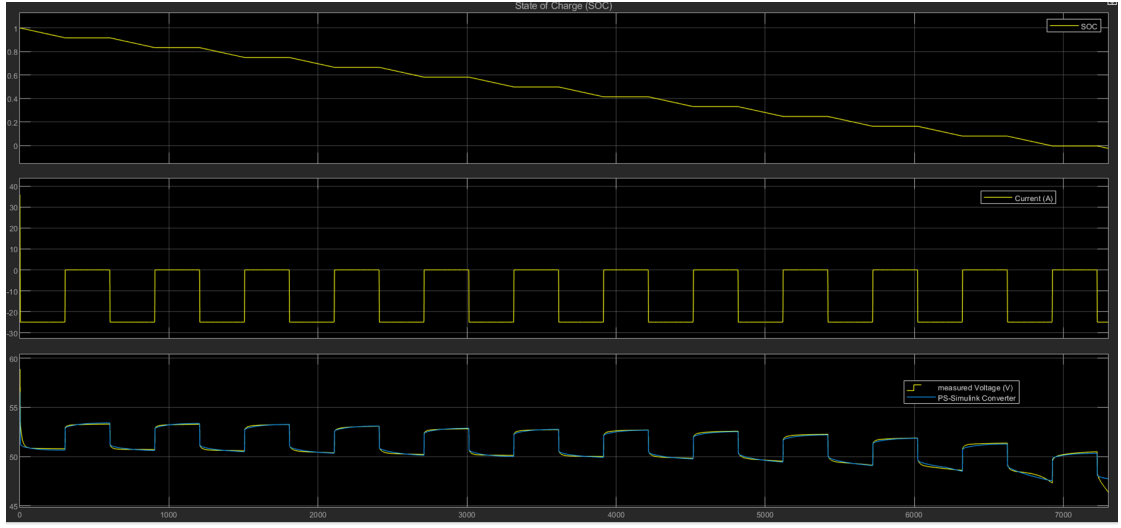


Figure 3.22: Pulse test results

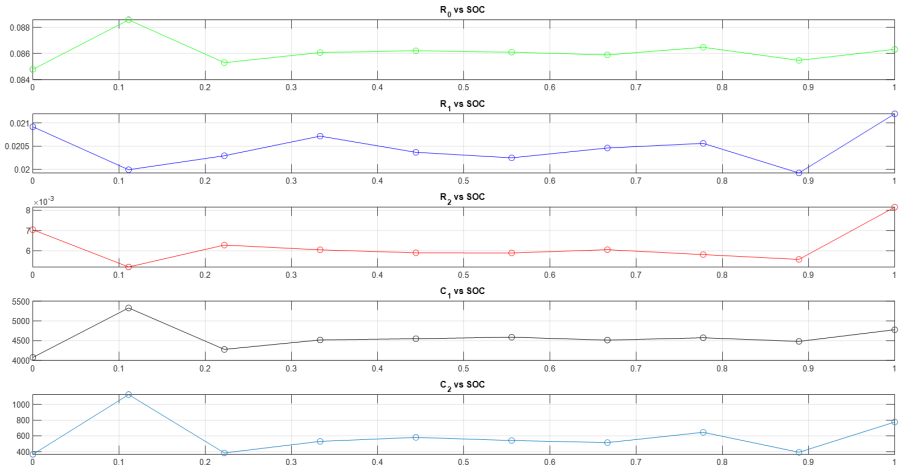


Figure 3.23: parameters values vs State of Charge

make a digression on how the Simulink Design optimization works to characterize the parameters.

3.3.6 Optimization problem formulation

When you perform parameter estimation, the software formulates an optimization problem. The optimization problem solution is the estimated parameter values set

[16]. This optimization problem consists of:

- x design variables: The model parameters and initial states to be estimated.
- $F(x)$ objective function: A function that calculates a measure of the difference between the simulated and measured responses. Also called cost function or estimation error.
- *Bounds*: Limits on the estimated parameter values.

The optimization solver tunes the values of the design variables to satisfy the specified objectives and constraints. The exact formulation of the optimization depends on the optimization method that you use.

The software tunes the model parameters to obtain a simulated response (y_{sim}) that tracks the measured response or reference signal (y_{ref}). To do so, the solver minimizes the cost function or estimation error $e(t) = y_{ref}(t) - y_{sim}(t)$, a measure of the difference between the simulated and measured responses.

The optimization method chosen in this thesis is the Nonlinear Least Squares, which minimizes the squares of the residuals and it's the recommended method for parameter estimation. This method requires a vector of error residuals, computed using a fixed time base. Do not use this approach if you have a scalar cost function or if the number of error residuals can change from one iteration to another.

The Optimization problem formulation is:

$$\begin{cases} \min_x \|F(x)\|_2^2 = \min_x (f_1(x)^2 + f_2(x)^2 + \dots + f_n(x)^2) \\ \text{s.t. } \underline{x} < x < \bar{x} \end{cases} \quad (3.2)$$

3.3.7 Thermal model and its parameters estimation

In this thesis, the battery is considered as a single homogeneous layer and the heat is generated in the centre of the battery and flows towards the surface, where it can be measured by the thermocouples shown in figure 3.4. For this modelling purpose, reversible and irreversible heat in the cell is considered. Irreversible heat consists of the Joule heating effect due to internal resistance of the cell, for instance these values are then calculated with sufficient electrical battery model and evaluated both offline and in real time calculation. Reversible heat is a result of entropy effect which can be negative or a positive value depending on the direction of current flow during charging and discharging process of the battery. Other heat transfer

mechanism such as conductive heat transfer and convective heat transfer are also included into the model.

Heat generation mechanism: As written above, the irreversible heat consists of the Joule effect due to the internal resistances in the cell. Based on the electric model approach of the cell as shown in figure 3.19, three main resistances are considered in this work: the polarization resistances (R_1, R_2) and the Ohmic resistance (R_0).

The equation for the heat generated at a central point in the cell is:

$$Q_{joule} = R_0 i^2 + R_1 i^2 + R_2 i^2 \quad (3.3)$$

As demonstrated in [17]. The reversible heat generation mechanism consists of the entropy effect can be negative or positive depending on charging or discharging process. Based on measurement of a 25 Ah cell the initial model parameters have been optimized with Recursive Least Square (RLS) method. The obtained results show that the estimated values of internal resistance, capacity, OCV and others provide valuable information about battery internal/external temperature and terminal voltages even if the physical sensors become faulty and go out of operation for any reason. The heat generated by the entropy variation depends strongly on the OCV and therefore the SOC. The equation for the reversible heat can be written as:

$$Q_{rev} = -T \Delta S \frac{i}{nF} \quad (3.4)$$

Thus the total heat is given by:

$$Q_{tot} = Q_{joule} + Q_{rev} \quad (3.5)$$

Heat Transfer Effects

- Conductive heat transfer:

$$Q_{cond} = \frac{kA}{d}(T_i - T_{battery}) \quad (3.6)$$

Where k is the thermal conductivity, A is the cross section area of the battery,

d is the battery thickness, T_i the battery estimated internal temperature and $T_{battery}$ Temperature on the surface of the battery.

- Convective heat transfer:

$$Q_{conv} = hA(T_{battery} - T_{amb}) \quad (3.7)$$

h is the Heat transfer coefficient and T_{amb} is the ambient temperature.

The Mathematical formulation of the battery thermal model is given by:

$$c_p m \frac{dT_i}{dt} = Q_{tot} - \frac{kA}{d}(T_i - T_{battery}) \quad (3.8)$$

Considering that the amount of heat flow absorbed by conduction effect is the same as the one absorbed by convection. We can write: $Q_{cond} = Q_{conv}$. From this equation, we can derive the relation between T_{amb} and T_i :

$$T_{battery} = \frac{kT_i + hDT_{amb}}{hd + k} \quad (3.9)$$

Parameters k , h and C_p will be identified by training the data with real measurements. All necessary heat coefficients are brought in table ??.

The mathematical model has been designed in Simscape as represented in figure:

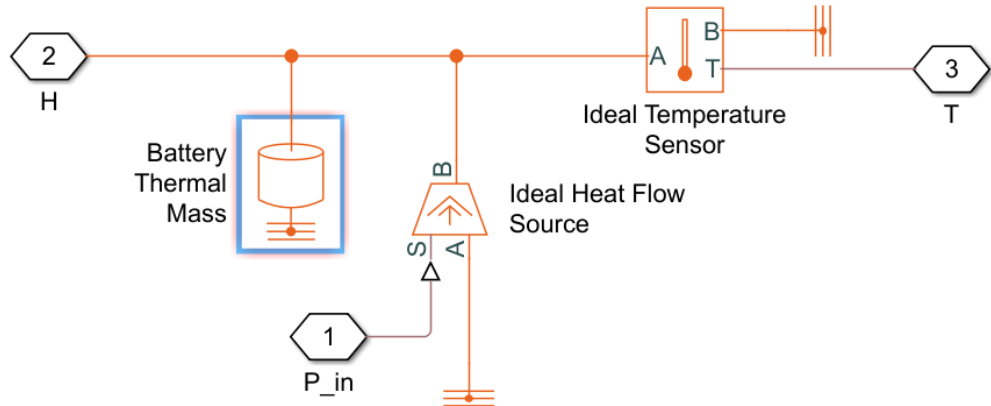


Figure 3.24: Thermal model developed in Simscape

Test for thermal parameters estimation This test is used to experimentally determine the values of k , h and C_p . It consists in going charge and discharge the battery, at the nominal current of 1 C, equal to 25 A. When the cut-off is reached, the discharge is interrupted and the battery is rest. During the test the battery temperature is measured and in particular the battery's temperature trend is observed since the current step ceases. The test is carried out at the ambient temperature which is constant for the whole test. The basic idea is to heat the battery internally and then observe how it releases the heat to the outside, supposed to be an ideal heat sink, and obtain the values of its parameters that come into play in the thermal equation 3.9 in which the environment is assumed to be at a constant temperature and the thermal power produced internally zero.

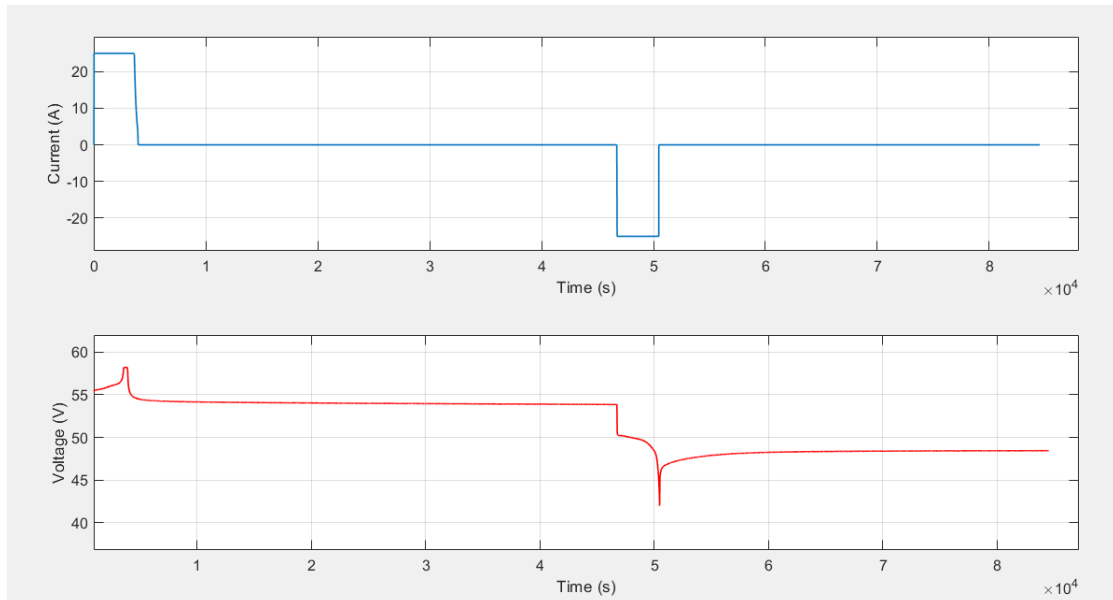


Figure 3.25: Current and Voltage profile for thermal parameters estimation

using the same optimization procedure, by means of simulink design optimization software, seen for the electrical parameters in 3.3.5 we obtained:

The battery thermal parameters obtained are shown in table ??

3.3.8 Final parameter estimation

Taking up what was introduced in the section 3.3.5, now we pose the problem of characterizing the entire look up table, thus for the 10 values of SOC and for the 3 values

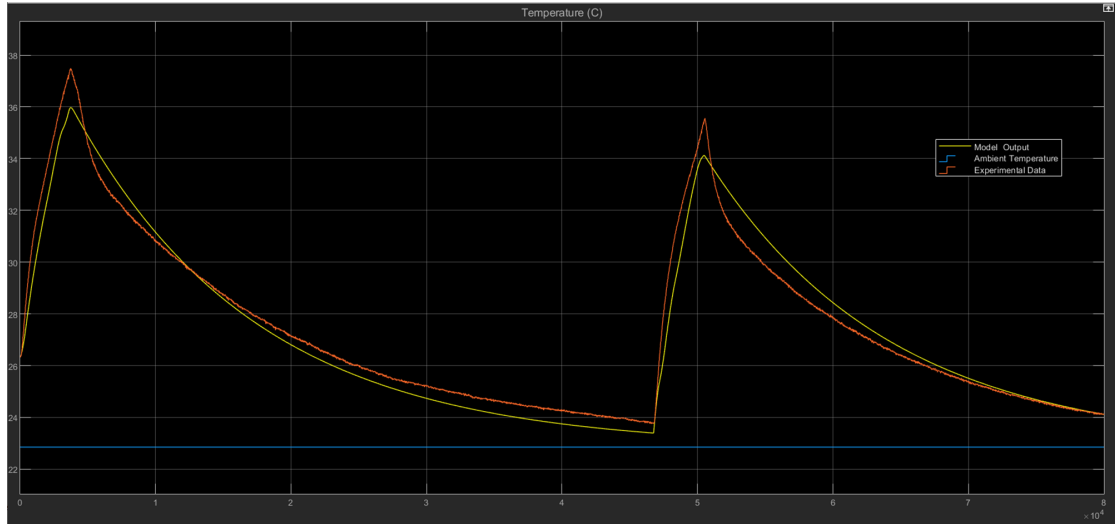


Figure 3.26: Temperature measured vs simulated

Estimated heat coefficient of the battery			
Parameter	Thermal resistance	Heat transfer coefficient	Specific heat capacity
Sign	$k \left(\frac{K}{W} \right)$	$h \left(\frac{W}{m^2 K} \right)$	$C_p \left(\frac{J}{kg/K} \right)$
Value	0.279	15.841	1166.5

Table 3.3: Thermal parameters

of working temperature of the battery, for all parameters: $E_m, R_0, R_1, C_1, R_2, C_2$. In order to make the optimization algorithm work better and not get trapped in local minimums we take as starting point for the parameters the values obtained from the previous estimate depending only on SOC. The estimation procedure for the lookup tables is shown in figure 3.27

And the parameters obtained are represented in the following plots, each with its corresponding lookup table:

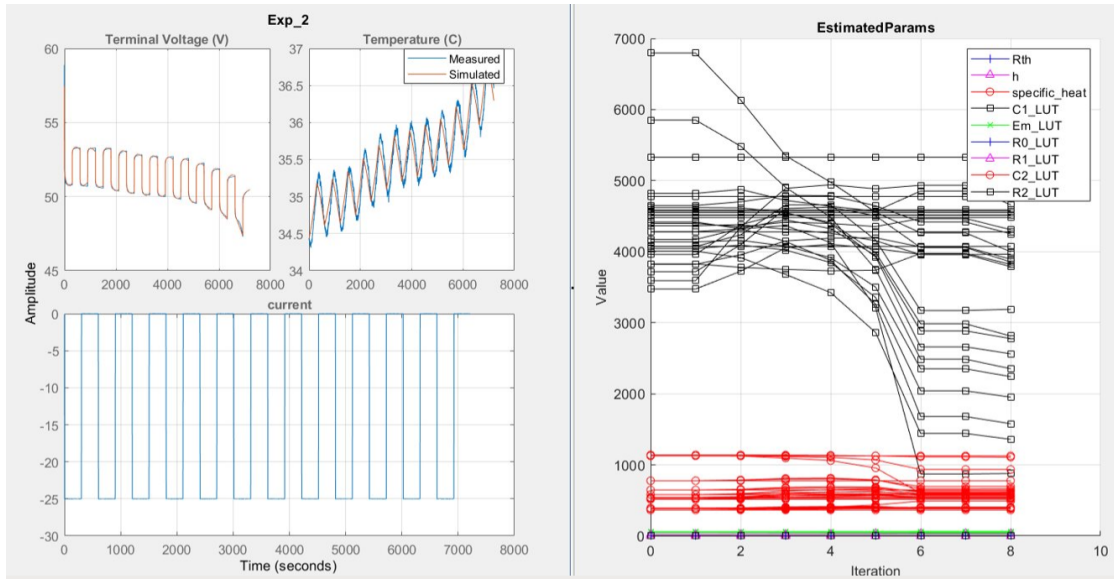
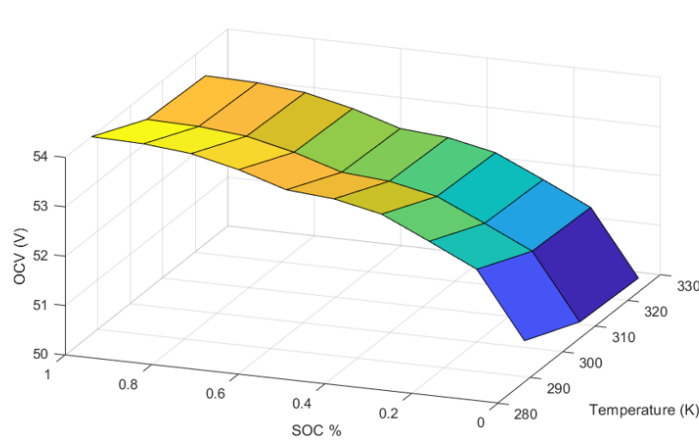


Figure 3.27: Final parameter estimation with simulink design optimization



	25 °C	35 °C	45°C
0.1	50.842	50.3390	50.2887
0.2	52.180	51.6640	51.6123
0.3	52.640	52.1190	52.0669
0.4	53.082	52.5570	52.5044
0.5	53.283	52.7560	52.7032
0.6	53.359	52.8310	52.7782
0.7	53.659	53.1280	53.0749
0.8	53.877	53.3440	53.2907
0.9	53.968	53.4340	53.3806
1	53.994	53.4600	53.4065

Figure 3.28: Open circuit voltage lookup table

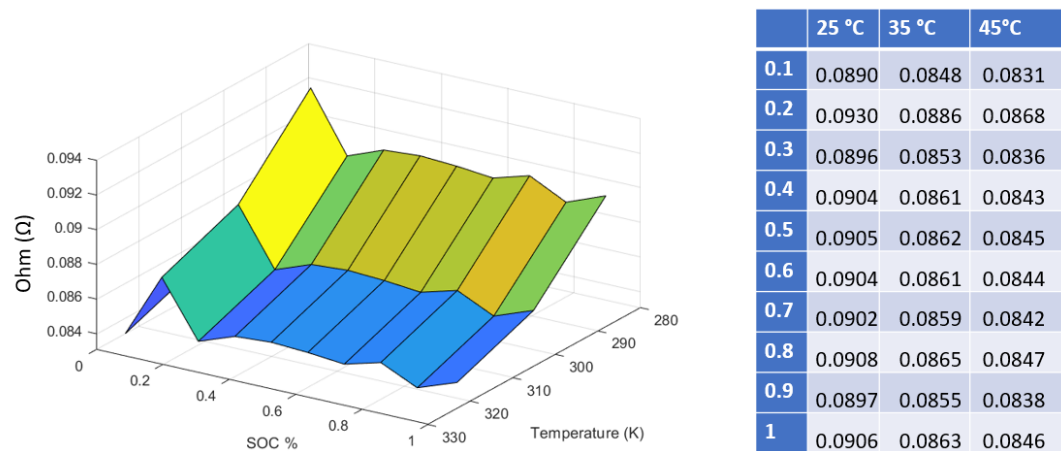


Figure 3.29: Internal resistance lookup table

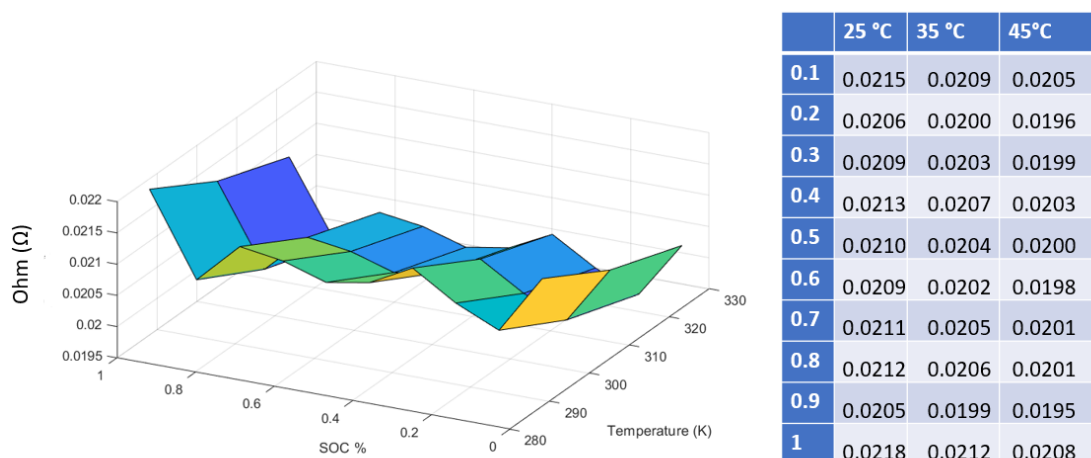
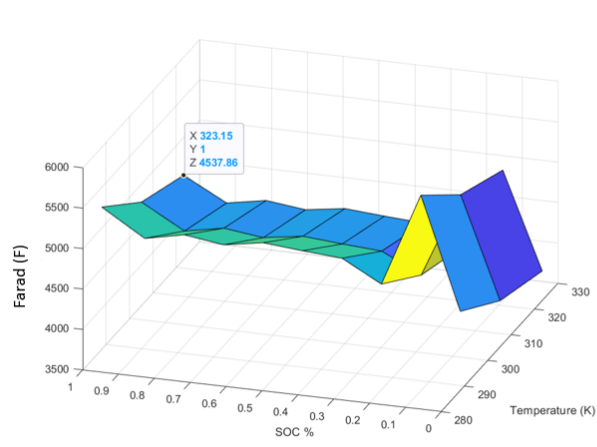


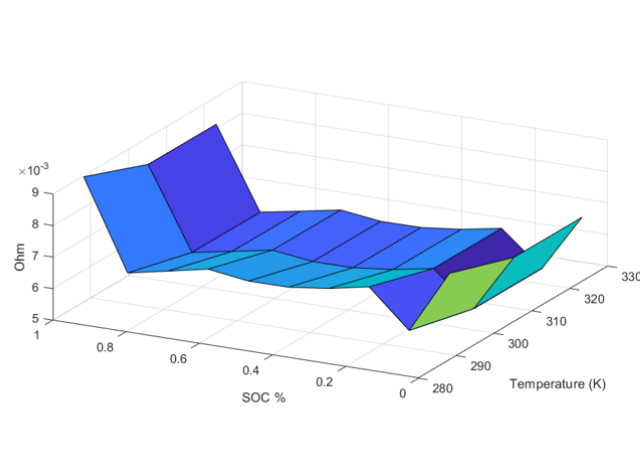
Figure 3.30: R_1 resistance lookup table



	25 °C	35 °C	45°C
0.1	4.4825	4.0750	3.8712
0.2	5.8617	5.3288	5.0624
0.3	4.7058	4.2780	4.0641
0.4	4.9689	4.5172	4.2913
0.5	5.0043	4.5494	4.3219
0.6	5.0464	4.5876	4.3582
0.7	4.9641	4.5128	4.2872
0.8	5.0304	4.5731	4.3444
0.9	4.9288	4.4807	4.2567
1	5.2544	4.7767	4.5379

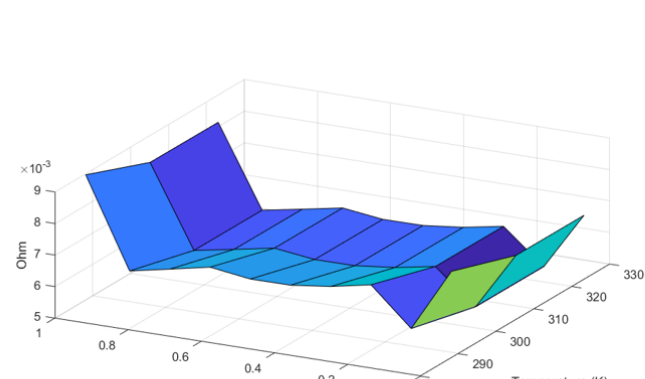
*10e3

Figure 3.31: R_1 capacitance lookup table



	25 °C	35 °C	45°C
0.1	0.0077	0.0070	0.0070
0.2	0.0057	0.0052	0.0052
0.3	0.0069	0.0063	0.0063
0.4	0.0067	0.0061	0.0060
0.5	0.0065	0.0059	0.0059
0.6	0.0065	0.0059	0.0059
0.7	0.0067	0.0061	0.0061
0.8	0.0064	0.0058	0.0058
0.9	0.0061	0.0056	0.0056
1	0.0090	0.0081	0.0081

Figure 3.32: R_2 resistance lookup table



	25 °C	35 °C	45°C
0.1	0.0077	0.0070	0.0070
0.2	0.0057	0.0052	0.0052
0.3	0.0069	0.0063	0.0063
0.4	0.0067	0.0061	0.0060
0.5	0.0065	0.0059	0.0059
0.6	0.0065	0.0059	0.0059
0.7	0.0067	0.0061	0.0061
0.8	0.0064	0.0058	0.0058
0.9	0.0061	0.0056	0.0056
1	0.0090	0.0081	0.0081

Figure 3.33: C_2 capacitance lookup table

From the data obtained it can be deduced that the *OCV* characteristic is an increasing monotonic function of a non-linear nature of the state of charge. The next parameter that is analyzed is the resistor R_0 which takes care of representing the phenomenon of the ohmic jump. The figure 3.29 shows the experimental results for one of the tested cells. As can be seen, the trend as a function of the state of charge is non-linear in nature, especially at low temperatures, and in general the resistance, with the same state of charge, decreases with increasing temperature. This behavior can be explained physically by referring again to the concept of ionic conductivity. In fact, there are various conduction mechanisms, and it is reasonable to think that the overall resistance is largely due to the electrolyte, essentially ionic conductor, rather than to the electrodes, characterized by a mainly electronic conductivity. The conductivity of the electrolyte is therefore mainly dependent on the mobility of the ions, which increases with increasing temperature, and decreases with decreasing temperature, linked to the electronic mobility, of the electrodes. It is also noted that for low values of the relative state of charge there is a marked increase in the resistance R_0 . This increase may be due to the fact that in this situation most of the charge carriers have now migrated from the anode to the cathode and therefore there are no more carriers available, which precisely leads to an increase in resistance. Furthermore, it is noted that this increase in resistance R_0 at low temperatures begins to manifest itself even for not particularly low values of the relative state of charge, while at high temperatures this happens when the cell is already almost discharged. This may be due to the fact that at low temperatures, due to the reduced ionic mobility, the number of carriers is lower and therefore runs out earlier than in the case of operating at high temperatures. From the behavior shown by R_0 as the temperature varies, it is therefore now possible to understand the trend of the *OCV* in Figure 3.28. In fact, as the temperature decreases, R_0 increases and therefore the consequent associated ohmic jump. With the same no-load voltage and current, the limit voltage is thus reached earlier than occurs at high temperatures, resulting in a lower discharge capacity. The trend of the remaining resistive parameters will also exhibit similar behaviors.

The experimental results obtained for the parallel RC groups, placed in series with R_0 , of the model are illustrated in the following figures: 3.30, 3.31, 3.32, 3.39. These groups are responsible for representing the phenomenon of the recovery effect. The trend of the time constant associated with these RC groups presents a very particular behaviour. Globally, however, it can be stated that the time constants associated with these RC group tend to decrease with increasing temperature. It

can be assumed that this is due to the greater ionic mobility at high temperatures, which allows for faster internal dynamics. The fact of having such irregular trends of the time constant may be due to the fact that it cannot be attributed a precise physical meaning, as is the case for R_1 or R_2 (which follow the same trend as R_0), but only to associate the idea of dynamic speed with which the recovery effect occurs. In fact, its value has been calculated as the value that minimizes the squared error between the voltage transient described by the RC groups and the observed one, which will have a trend that can deviate even significantly from one of the exponential type such as that of the objective function.

3.3.9 Model verification

In this section, the accuracy of the proposed temperature-dependent second-order RC equivalent circuit model is verified. The identified parameters obtained from section 3.3.8 are employed in the proposed model in figure 3.19, and the model accuracy is evaluated in terms of the difference (error) between the measured terminal voltage and that resulting from the proposed model. For verification purposes, the model has undergone the discharging test, charging test, RW and WLTP, under varying internal temperature conditions but with a constant ambient temperature. The voltages resulting from the model as well as the voltage errors are plotted in Figure 3.36 and 3.37, under a constant ambient temperature of 23 °C. It is shown that for the discharging test, the model output voltages are very close to the measured terminal voltages, and the voltage errors are maintained within ± 20 mV. As for the WLTP, the model output voltage follows the measured voltage very well, with a slightly increased error magnitude compared with the first two cases. Note that the error is still maintained within a very small range and the moving average of the error is very close to 0.

From the data obtained it can be deduced that the E_m characteristic is an increasing monotonic function of a non-linear nature of the state of charge. The next parameter that is analyzed is the resistor R_0 which takes care of representing the phenomenon of the ohmic jump. The figure shows the experimental results for one of the tested cells.

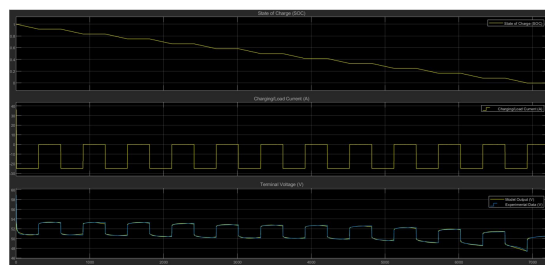


Figure 3.34: Voltage model output vs experimental data

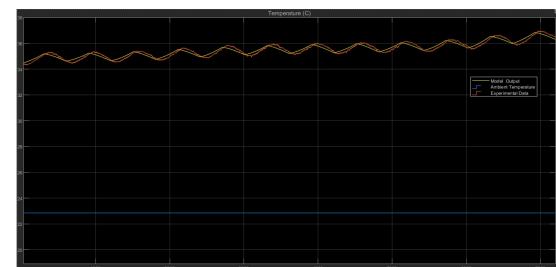


Figure 3.35: Temperature model output vs data

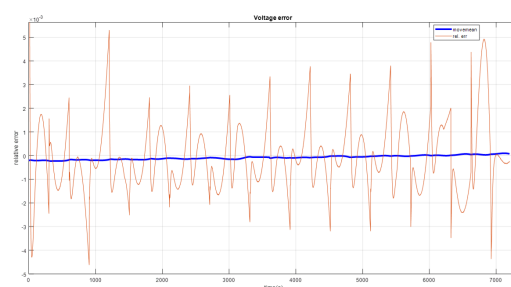


Figure 3.36: Voltage's error

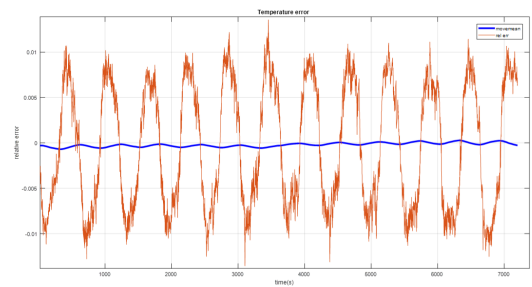


Figure 3.37: Temperature's error

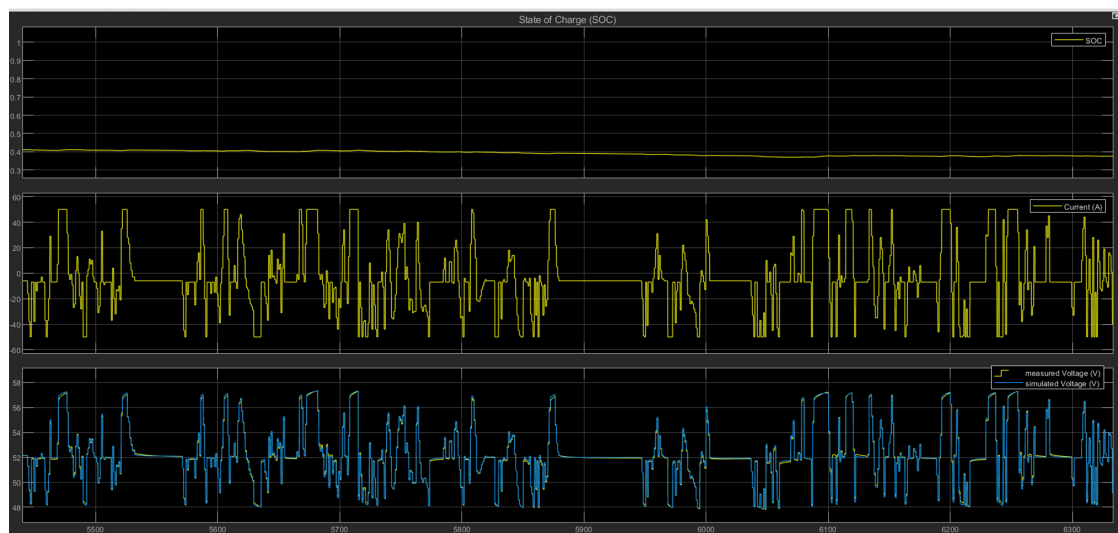


Figure 3.38: Model tested on a WLTP profile

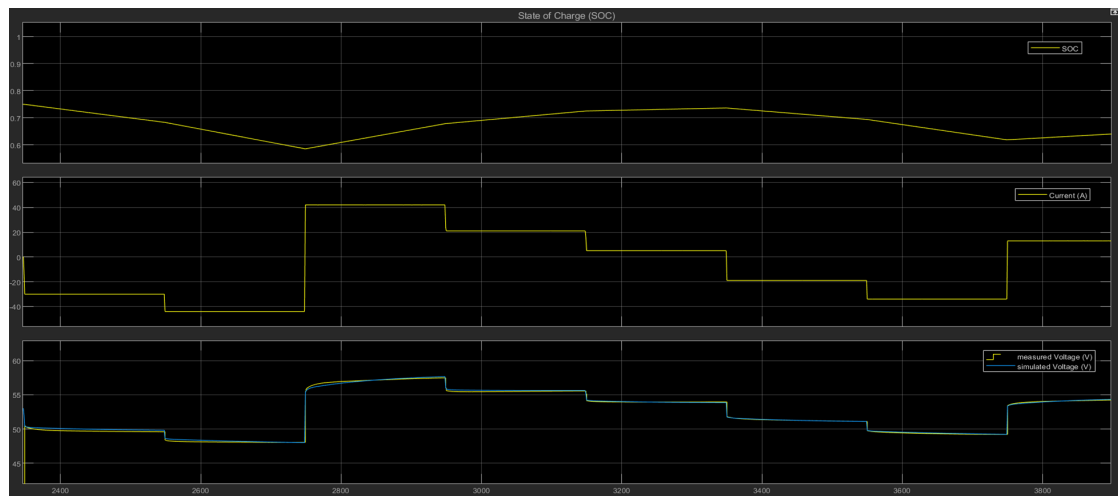


Figure 3.39: Model tested on a RW profile

Chapter 4

Complete model and SOC estimation by means of UKF

The performance of battery determine the performance of the mild hybrid electric vehicle in terms of driving consumption. And the accuracy of the estimated State of charge (SOC) is the most important key technique to ensure the normal application of the battery pack. People are increasingly demanding on the accuracy of the estimated SOC on the MHEV power battery. AS described in chapter 3, the battery itself has highly nonlinear characteristics and this characteristic can be intensified in the working environment of unstable current and unstable temperature, which will make it difficult to estimate SOC accurately.

A number of methods are used to estimate the battery SOC, such as ampere-hour, integral method, open circuit voltage method, the internal impedance method, neural network, Kalman filter algorithm, unscented Kalman filter, particle filter, and other nonlinear observers. Compared with the Ah integral method or open circuit voltage method, a closed-loop SOC estimation method based filter is attracting more attentions, Kalman filtering algorithm can be used for various state estimation of the battery. And the algorithm is only applicable to linear system, but the Li-ion battery model is nonlinear; Unscented Kalman filter (Unscented Kalman Filtering, UKF) as a kind of special estimation method is proposed for nonlinear systems, and it has obtained the rapid development in recent years [18].

4.1 UKF

4.1.1 What is an Unscented Kalman Filter?

The Unscented Kalman Filter (UKF) is an algorithm, that has an alternative way to estimate the state of a nonlinear system, doesn't use the first order Taylor expansion. The UKF addresses the approximation problem of the EKF (Extended Kalman filter [19]) by introducing the concept of weighted sigma points, which are deterministically selected from the a Gaussian approximation [20]. The sigma points are chosen so that their mean and covariance are exactly x_{k-1}^a and P_{k-1} . Each sigma point is then propagated through the system state function to yield new sigma points. The newly estimated mean and covariance are then computed based on their statistics. This process is called the unscented transformation. Consider the system that demonstrates how a Markov process works 4.1

$$\begin{cases} x_k = f(x_{k-1}, u_k) + v_k \\ z_k = h(x_k, u_k) + w_k \end{cases} \quad (4.1)$$

where x_k is the system state vector; u_k is the known input vector; and z_k is the measurement vector at time step k . Correspondingly, $f()$ and $h()$ are the state function and the measurement function, respectively, and they can be either linear or nonlinear; v_k and w_k are the process Gaussian noise and the measurement Gaussian noise with zero-means and covariances Q and S , respectively. Specifically, $v_k \sim N(0, Q)$, and $w_k \sim N(0, S)$. Let n be the dimension of the state vector. To apply the UKF, $2n + 1$ sigma points with weights x_k^i, W_i , $i = 1 : 2n + 1$ are generated according to 4.2

$$\begin{cases} x_{k-1}^0 = x_{k-1}^a, \\ x_{k-1}^i = x_{k-1}^a + \sqrt{n + \lambda} [\sqrt{P_{k-1}}]_i, \\ x_{k-1}^{i+n} = x_{k-1}^a + \sqrt{n + \lambda} [\sqrt{P_{k-1}}]_i, \quad i = 1 : n \end{cases} \quad (4.2)$$

Each sigma point is then propagated trough the non linear state function 4.3

$$x_k^{i,f} = f(x_{k-1}^i, u_k), \quad i = 0, \dots, 2n, \quad (4.3)$$

The mean and the covariance of x_k^f is then computed via equations 4.4 and 4.5

$$x_k^f = \sum_{i=0}^{2n} W_i^m x_k^{i,f} \quad (4.4)$$

$$P_k^f = \sum_{i=0}^{2n} W_i^c (x_k^{i,f} - x_k^f) (x_k^{i,f} - x_k^f)^T + Q \quad (4.5)$$

where W_i^m and W_i^c are respectively defined as:

$$\begin{cases} W_0^m = \frac{\lambda}{\lambda+n} \\ W_0^c = \frac{\lambda}{\lambda+n} + (1 - \alpha^2 + \beta) \\ W_i^m = \frac{1}{2(\lambda+n)}, \quad i = 1, \dots, 2n \\ W_i^c = \frac{1}{2(\lambda+n)}, \quad i = 1, \dots, 2n \end{cases} \quad (4.6)$$

where β controls the prior information of x_{k-1} . α and β are empirically set to default values 1 and 0, respectively; In other words, the spread of the the sigma points x_{k-1}^a is far from the mean vector x_{k-1}^a

Similarly the sigma points are propagated trough the measurement function:

$$z_k^{i,f} = h(x_k^{i,f}, u_k), \quad i = 0, \dots, 2n \quad (4.7)$$

The mean and the covariance of the z_k^f are then computed:

$$z_k^f = \sum_{i=0}^{2n} W_i^m z_k^{i,f} \quad (4.8)$$

The cross-covariance of the state and measurement is:

$$cov(x_k^f, z_k^f) = \sum_{i=0}^{2n} W_i (x_k^{i,f} - x_k^f) (x_k^{i,f} - z_k^f)^T \quad (4.9)$$

The kalman gain is computed as:

$$K_k = cov(x_k^f, z_k^f) cov(z_k^f)^{-1} \quad (4.10)$$

Thus, the state estimation can be obtained by:

$$x_k^a = x_k^f + K_k (z_k - z_k^f) \quad (4.11)$$

and the covariance can be updated by:

$$P_k = P_k^f - K_k cov(z_k^f) K_k^T \quad (4.12)$$

4.1.2 UKF for SOC estimation

As said before, an accurate estimation of the SOC is of crucial importance in a Battery management system (BMS) for a variety of reasons, and an advanced approach in estimating the SOC is the use of an observer, typically a UKF which receives the input and output signals from the battery and computes the internal states using the model of the battery, presented in 3.3.5, and a recursive algorithm.

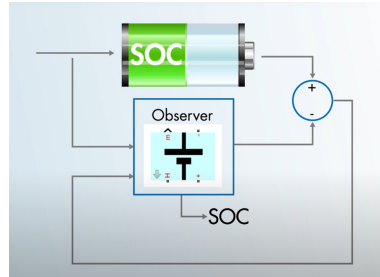


Figure 4.1: SOC estimation scheme

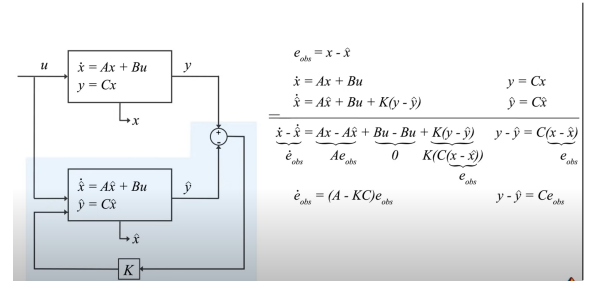


Figure 4.2: Observer

Thus, the UKF block from the simulink control system toolbox has been implemented in the model for SOC estimation. The UKF requires a minimum of 2 functions as arguments: a state transition function and a measurements function. These functions has been implemented as simulink bloks shown in figure 4.3.

The state Transition Function calculates the evolution of the states based on the current input, these calculations require the previous computation of the equivalent circuit parameters, using the temperature and current signals, that go through the non-linear lookup tables that characterize the battery (estimated using an optimization algorithm as described in chapter 3). While the measurement Function computes the terminal voltage as the difference between OCV and sum of individual voltage drops across of the rest of the equivalent circuit elements (2RC branches).

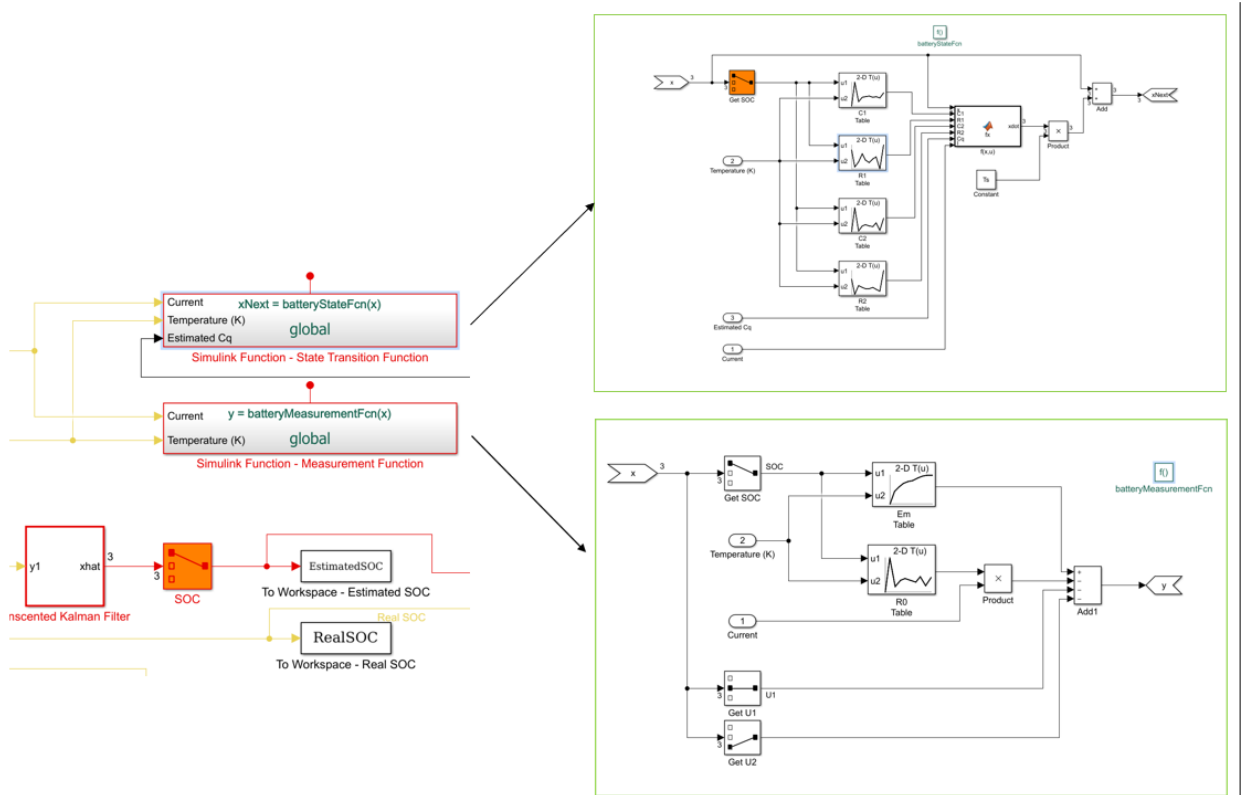


Figure 4.3: State transition function and measurement function

In our model the State vector of the battery is given by:

$$x(t) = \begin{pmatrix} SOC(t) \\ U_1(t) \\ U_2(t) \end{pmatrix} \quad (4.13)$$

And the state transition equation and measurement equation for the battery are:

$$\frac{d}{dt} \begin{pmatrix} SOC \\ U_1(t) \\ U_2(t) \end{pmatrix} = \begin{pmatrix} 0 \\ -\frac{1}{R_1(SOC,T)C_1(SOC,T)}U_1 \\ -\frac{1}{R_2(SOC,T)C_2(SOC,T)}U_2 \end{pmatrix} + \begin{pmatrix} -\frac{1}{3600} * C_q \\ \frac{1}{C_1(SOC,T)} \\ \frac{1}{C_2(SOC,T)} \end{pmatrix} I + W \quad (4.14)$$

$$E = E_m(SOC, T) - U_1 - U_2 - IR_0(SOC, T) + V \quad (4.15)$$

Since the UKF is a Discrete time filter (DT) we have to apply the Euler discretization. Let the sampling time be T_s . For a general nonlinear system $\dot{x} = f(x, u)$, the system can be discretized as:

$$x_{T+1} = x_T + f(x_T, u_T) * T_s$$

The state vector of the nonlinear battery system in DT is:

$$x_T = \begin{pmatrix} SOC_T \\ U_{1T} \\ U_{2T} \end{pmatrix}$$

Applying Euler discretization to 4.14 we have:

$$\begin{pmatrix} SOC(t+1) \\ U_1(t+1) \\ U_2(t+2) \end{pmatrix} = \begin{pmatrix} SOC(t) \\ U_1(t) \\ U_2(t) \end{pmatrix} + \begin{pmatrix} -\frac{1}{3600*C_q*I} \\ \frac{1}{C_1(SOC,T)} * I - \frac{1}{R_1(SOC,T)C_1(SOC,T)}U_1 \\ \frac{1}{C_2(SOC,T)}I - \frac{1}{R_2(SOC,T)C_2(SOC,T)}U_2 \end{pmatrix} T_s + W \quad (4.16)$$

The discretized state transition equation is implemented in the Simulink function named batteryStateFcn. The function input x_T is the state vector, and the function output x_{Next} is the state vector at the next step, calculated using the discretized

state transition equations. In the function, you need to specify the signal dimensions and data type of x_T and x_{Next} . In this example, the signal dimension for x_T and x_{Next} is 3, and the data type is double. Additional inputs to batteryStateFcn are the temperature, estimated capacity, and current. Note that the additional inputs are inputs to the state transition equations and are not required by the Unscented Kalman Filter block as shown in figure 4.4

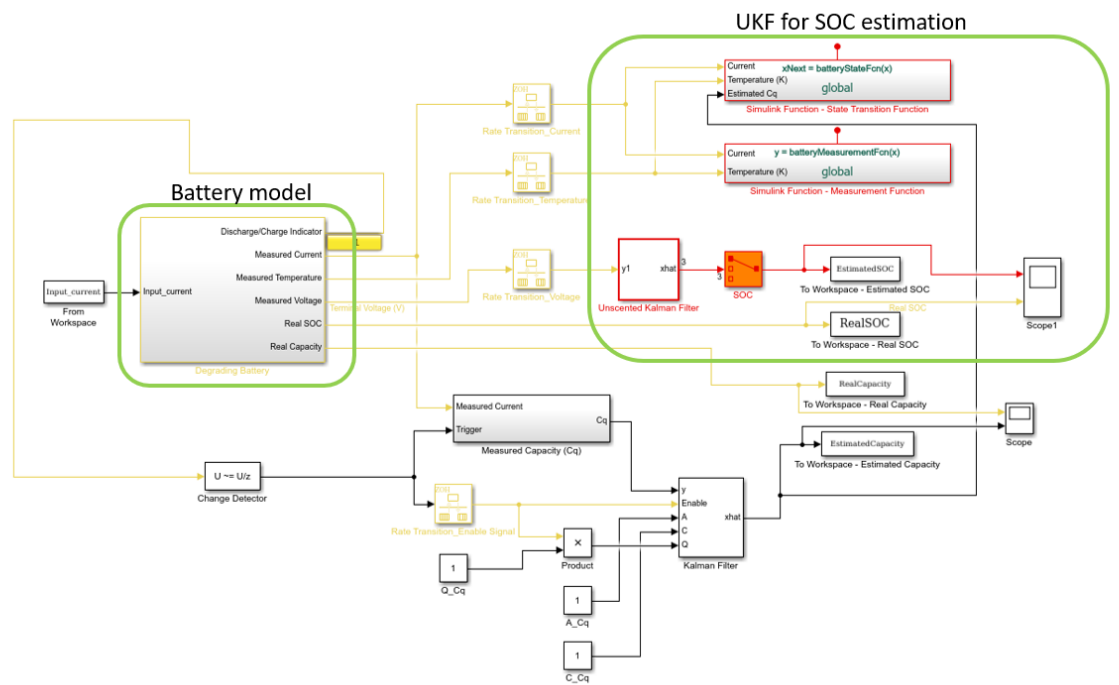


Figure 4.4: Complete model developed in Simulink

Finally, for the UKF the following parameters are specified:

- Time invariant covariance: $\begin{pmatrix} 2e-8 & 0 & 0 \\ 0 & 3e-7 & 0 \\ 0 & 0 & 3e-7 \end{pmatrix}$
- Initial covariance: $\begin{pmatrix} 0.01 & 0 & 0 \\ 0 & 1 & 0 \\ 0 & 0 & 1 \end{pmatrix}$

- Initial state: $\begin{pmatrix} 1 \\ 0 \\ 0 \end{pmatrix}$ The initial value for SOC is assumed to be 100 % (fully charged battery) while initial value for U_1 and U_2 is set to be 0, as we do not have any prior information of U_1 and U_2 .
- Unscented transformation parameters: $\alpha = 1$ determines the spread of sigma points around x. Set α to be 1 for larger spread; $\beta = 2$ is used to incorporate prior knowledge of the distribution. The nominal value for Beta is 2; $k = 0$, k is a secondary scaling parameter, its the nominal value is 0.

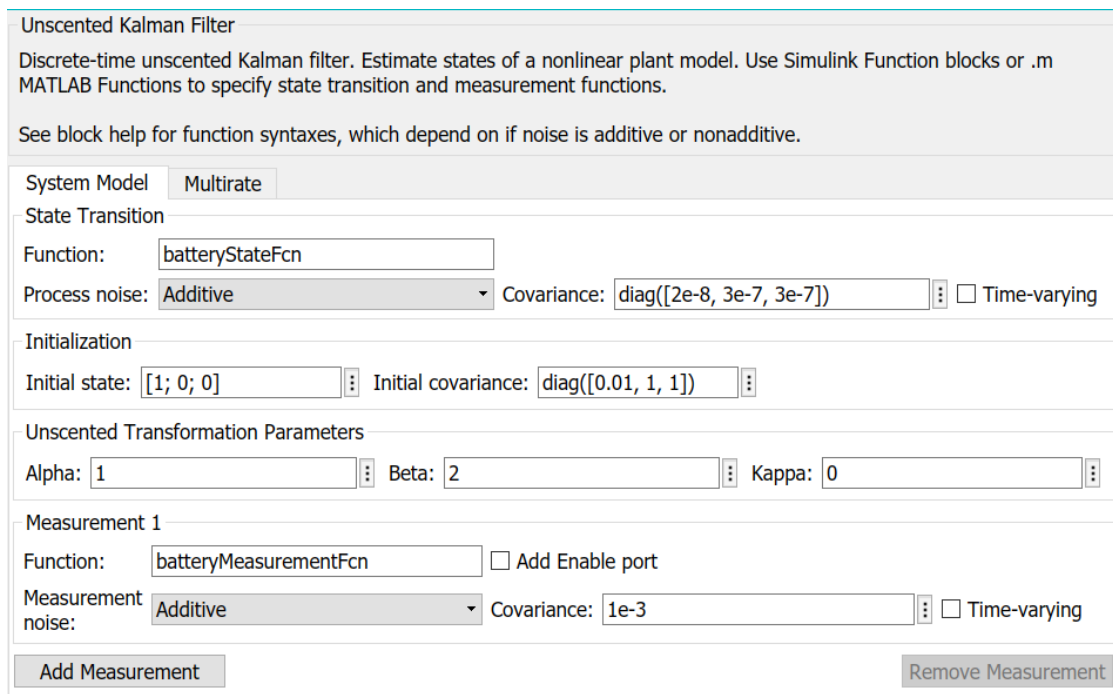


Figure 4.5: UKF parameters set up

4.1.3 SOC estimator validation

The model in figure 4.4 equipped with the UKF for the SOC estimation has been tested with a pulse and a WLTP profile in order to check it's correct behaviour. The results obtained with the relative errors are shown in the following plots: 4.7, 4.9

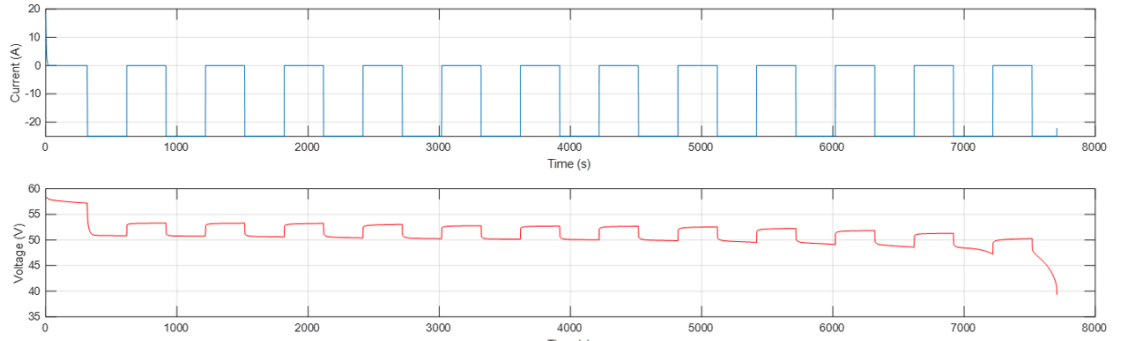


Figure 4.6: Pulse test current and voltage profile

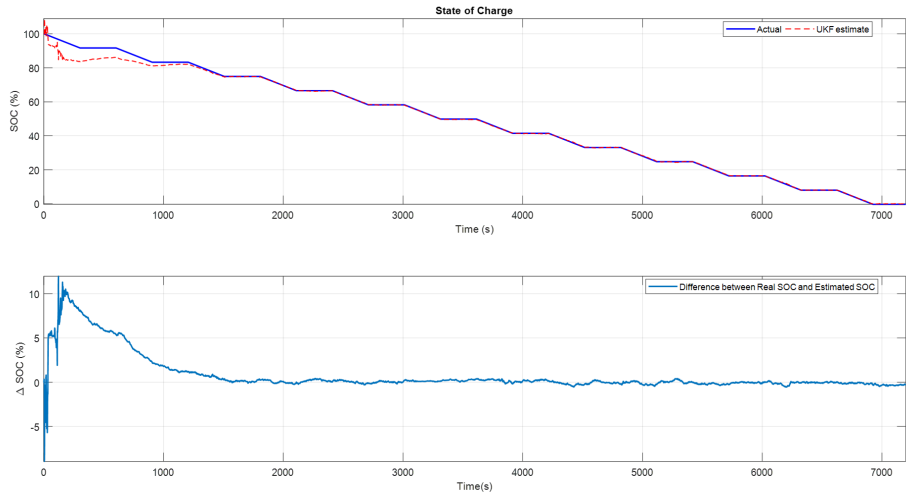


Figure 4.7: Pulse test real SOC vs UKF estimate

After an initial estimation error, the SOC converges quickly to the real SOC. The final estimation error is within 0.5% error. Thus, the Unscented Kalman Filter gives an accurate estimation of SOC.

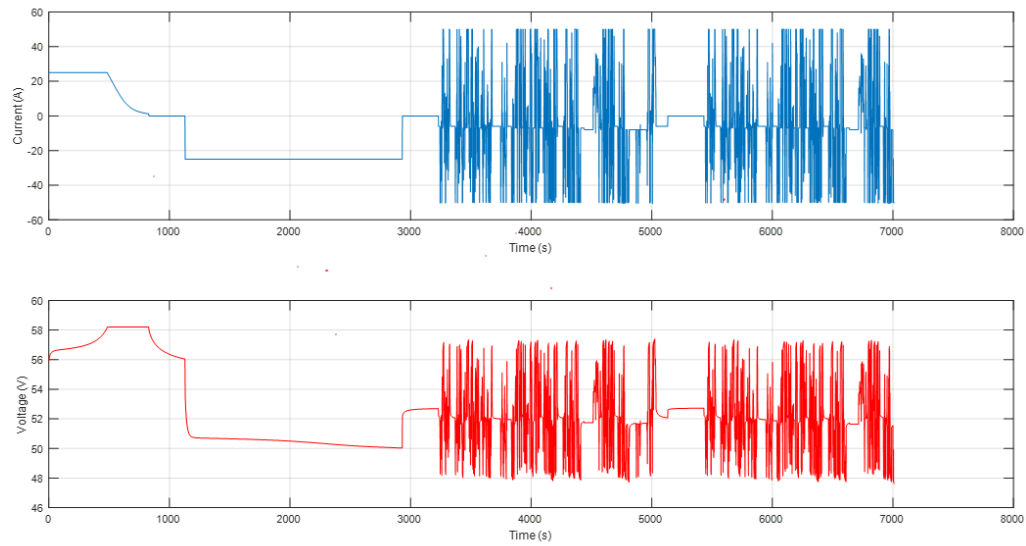


Figure 4.8: WLTP current and voltage profile

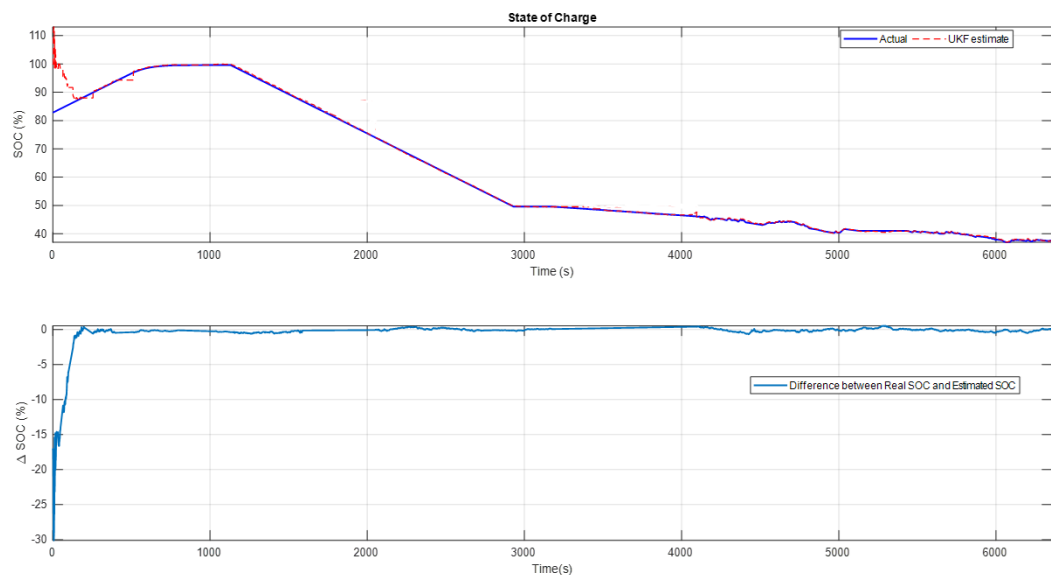


Figure 4.9: WLTP real SOC vs UKF estimate

4.1.4 SOH estimation

As introduced in 2.1.6 the state of health estimation (SOH) is a quite challenging task due many unknown and unpredictable factors influencing the health of the battery such as: operating temperature, uncertain driving condition, overcharging/discharging, high charge/discharge rate and improper charge/discharge cycles. In this model the battery degradation is simulated by decreasing the battery capacity C_q every charge/discharge cycle, using a threshold logic implemented in stateflow, (a simulink toolbox).

Since the degradation rate of capacity is not known in advance, set the state equation of C_q to a random walk:

$$C_{q_{k+1}} = C_{q_k} + W_{C_q}$$

where k is the number of discharge-charge cycles, and W_{C_q} is the process noise.

The battery is configured to automatically charge when the capacity is at 30% and switch to discharging when the capacity is 90%. Use this information to measure the battery capacity by integrating the current I over a charge or discharge cycle (coulomb counting).

The measurement equation for C_q is :

$$C_{q_k}^{measured} = C_{q_k} + V_{C_q} = \frac{\int_{t_{k-1}}^{t_k} Idt}{\Delta SOC_{nominal}} = \frac{\int_{t_{k-1}}^{t_k} Idt}{|0.9 - 0.3|} = \frac{\int_{t_{k-1}}^{t_k} Idt}{0.6} \quad (4.17)$$

where V_{C_q} is the measurement noise. The state transition and measurement equations of battery degradation can be put into the following state-space form:

$$C_{q_{k+1}} = A_{C_q} C_{q_k} + W_{C_q}$$

$$C_{q_k}^{Measured} = C_{C_q} C_{q_k} + V_{C_q}$$

where A_{C_q} and C_{C_q} are equal to 1.

For the above linear system, use a Kalman Filter to estimate battery capacity. The estimated C_q from the linear Kalman Filter is used to improve SOC estimation. In this work, an event-based linear Kalman filter is used to estimate C_q . Since C_q is measured once over a charge or discharge cycle, the linear Kalman Filter is

enabled only when charging or discharging ends.

At every discharge-charge transition, the battery capacity is estimated to improve the SOC estimation. The battery system outputs indicator signals to inform what process the battery is in. Discharging process is represented by -1 in the indicator signals while charging process is represented by 1. In this example, changes in the indicator signals are used to determine when to enable or disable Kalman Filter for capacity estimation.

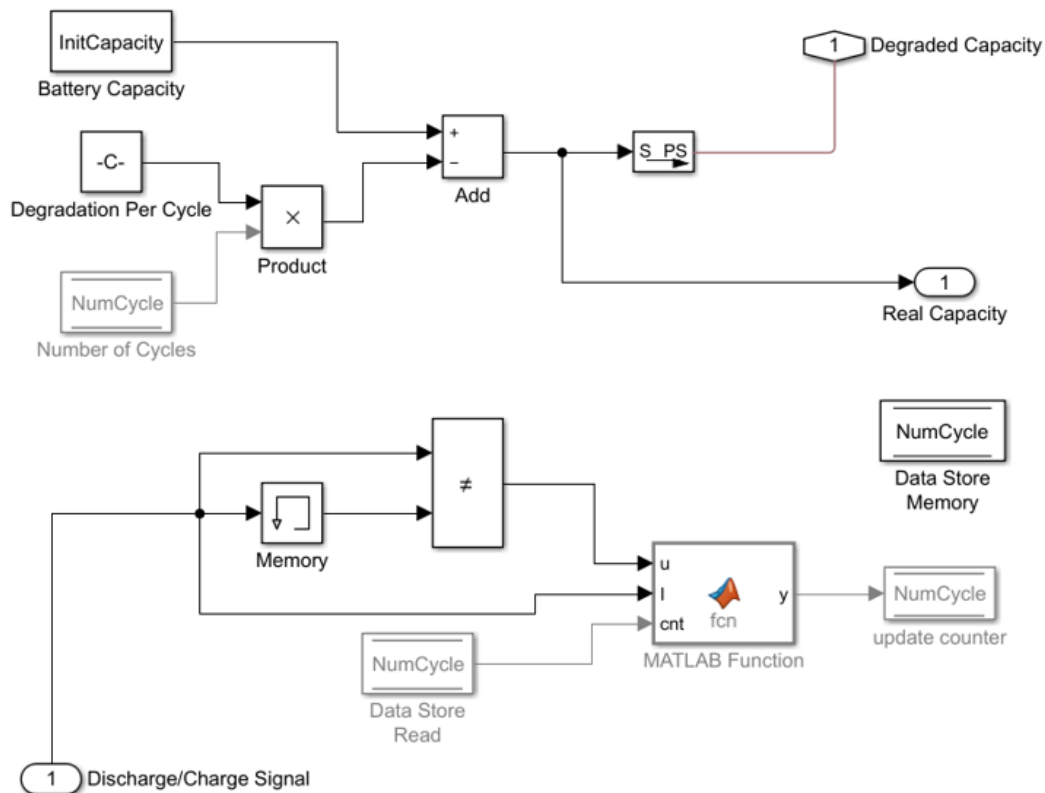


Figure 4.10: SOH estimation simulink scheme

In general, the Kalman Filter is able to track the real capacity. There is half cycle delay between estimated capacity and real capacity. This is because the battery capacity degradation happens when one full discharge-charge cycle ends. While the coulomb counting gives a capacity measurement of the last discharge or charge cycle.

Chapter 5

Conclusions and future development

The battery electrical characteristics are dependent on the ambient temperature; however, most existing battery equivalent circuit models have not taken into account the influences of ambient temperature.

In this thesis work, a temperature-dependent second-order RC equivalent circuit model is established, based on the electrical characteristics of lithium-ion batteries at different ambient temperatures (25, 35, 45 °C). The activity was carried out according to the closed box approach, through which has been built an equivalent model starting from measurements made exclusively at the external terminals of the battery by means of a cycler, a data logger, a battery tester and a specific software. The unknown model parameters were firstly obtained in using a physical approach that describes how the battery responds to current stimuli, in particular to a pulse. These parameters have been then used as starting point for the optimization of the model through a data fitting method by means of the simulink design optimization toolbox. Through this toolbox, that works as optimization solver which tunes the parameters to reduce the estimation error, it has been possible to find the best model parameters in order to have a behaviour as close as possible to the real battery, taking into account the working conditions (Temperature and SOC).

From the results obtained it has been possible to notice that the temperature is a determining factor in the functioning of a lithium-ion battery. In fact, the discharged capacity, given a certain current profile, does not depend only on this profile, but also on the temperature at which one is operating. Note that the

resistive parameters decrease in value as the temperature increases. The state of charge of the battery also influences these parameters, especially when it assumes low values, resulting in a sudden increase in resistance. These results therefore show that the main conduction mechanism that takes place in the battery is ionic in nature, although it is not the only one present. The trend of the capacitive parameters, on the other hand, does not have an equally unique behavior. This is due to the fact that it is not possible to associate a precise physical meaning to the capacities. However, in general it is observed that the internal dynamics become more rapid as the temperature rises.

Furthermore, the parameters obtained were subsequently used in the model during the verification phase, where it has been possible to evaluate the margin of error between the model and the real data. It has been shown that for both the discharging and charging tests, the model errors are maintained within $\pm 30mV$. As for the WLTP, the accuracy of the model is reduced, but the error is still maintained within a very small range, that is, $\pm 50mV$. These verification results indicate that the proposed model provides not only accurate output voltage, but also good behaviour for temperature variations.

Moreover, the obtained model has been equipped with an UKF for SOC estimation, in order to have an internal feedback loop to update parameter values based on charge status.

The results obtained have shown an error within 0.5% in estimating SOC, thus, the UKF is able to track to the real SOC quite accurately.

Finally, as far as concern the SOH estimation the proposed method consisted in the implementation of an event-based KF to estimate the capacity C_q and so to improve the SOC estimation by tracking the real capacity.

Future research developments on the subject will first have to analyze how the parameters vary as battery ages. Furthermore, it would be useful to establish if and in which way the deterioration of the cells is a function of the ambient temperature, as well as of the sustained work profiles. Another aspect to be addressed concerns the SOH estimator. The estimator based on a KF was approached only as a preliminary, without implementing a rigorous theoretical analysis, and further studies could identify how this estimator can be optimized according to the battery temperature and SOC. Furthermore, in the case of a battery, the estimator should also consider the thermal inhomogeneity between the cells, which implies the use in the model of a more complex thermal network than that presented in this work.

Finally, in the present work KF-based estimators of the state of charge have always been used. It would therefore be very useful to develop a state of charge estimator aimed at the user, which immediately communicates how much residual capacity is actually left through data driven approaches such as: Fuzzy Logic, Artificial Neural Networks and Support Vector Machine.

Bibliography

- [1] Mehrdad Ehsani, Krishna Veer Singh, Hari Om Bansal, and Ramin Tafazzoli Mehrjardi. «State of the art and trends in electric and hybrid electric vehicles». In: *Proceedings of the IEEE* 109.6 (2021), pp. 967–984 (cit. on p. 1).
- [2] Mehrdad Ehsani, Krishna Veer Singh, Hari Om Bansal, and Ramin Tafazzoli Mehrjardi. «State of the art and trends in electric and hybrid electric vehicles». In: *Proceedings of the IEEE* (2021) (cit. on p. 2).
- [3] SoDuk Lee, Jeff Cherry, Michael Safoutin, Joseph McDonald, and Michael Olechiw. «Modeling and validation of 48v mild hybrid lithium-ion battery pack». In: *SAE International Journal of Alternative Powertrains* 7.3 (2018), pp. 273–288 (cit. on p. 2).
- [4] Associazione nazionale per la protezione antincendio e altri. *NFPA 70: codice elettrico nazionale*. NationalFireProtectionAssoc, 2007 (cit. on p. 5).
- [5] «Voltage sag: una panoramica degli standard IEC e IEEE e criteri applicativi». In: *1999 IEEE Transmission and Distribution Conference (Cat. No. 99CH36333)*. Vol. 2. IEEE, 1999, pp. 585–589 (cit. on p. 5).
- [6] John Chiasson and Baskar Vairamohan. «Estimating the State of Charge of a Battery». In: () (cit. on p. 9).
- [7] Yongyao Xia, Yunhong Zhou, and Masaki Yoshio. «Capacity Fading on Cycling of 4 V Li / LiMn₂O₄ Cells». In: *Journal of The Electrochemical Society* 144.8 (Aug. 1997), pp. 2593–2600. DOI: 10.1149/1.1837870. URL: <https://doi.org/10.1149/1.1837870> (cit. on p. 9).
- [8] Prakash Venugopal et al. «State-of-Health estimation of li-ion batteries in electric vehicle using IndRNN under variable load condition». In: *Energies* 12.22 (2019), p. 4338 (cit. on p. 10).

- [9] Hongwen He, Rui Xiong, and Jinxin Fan. «Evaluation of lithium-ion battery equivalent circuit models for state of charge estimation by an experimental approach». In: *energies* 4.4 (2011), pp. 582–598 (cit. on p. 12).
- [10] Binyu Xiong, Jiyun Zhao, Zhongbao Wei, and Maria Skyllas-Kazacos. «Extended Kalman filter method for state of charge estimation of vanadium redox flow battery using thermal-dependent electrical model». In: *Journal of Power Sources* 262 (2014), pp. 50–61 (cit. on p. 19).
- [11] Yidan Xu, Minghui Hu, Chunyun Fu, Kaibin Cao, Zhong Su, and Zhong Yang. «State of Charge Estimation for Lithium-Ion Batteries Based on Temperature-Dependent Second-Order RC Model». In: *Electronics* 8.9 (2019). ISSN: 2079-9292. URL: <https://www.mdpi.com/2079-9292/8/9/1012> (cit. on p. 21).
- [12] Yidan Xu, Minghui Hu, Chunyun Fu, Kaibin Cao, Zhong Su, and Zhong Yang. «State of charge estimation for lithium-ion batteries based on temperature-dependent second-order RC model». In: *Electronics* 8.9 (2019), p. 1012 (cit. on p. 25).
- [13] Artur Kopczynski, Piotr Piórkowski, and Paweł Roszczyk. «Parameters selection of extended-range electric vehicle powered from supercapacitor pack based on laboratory and simulation tests». In: *IOP Conference Series: Materials Science and Engineering* 421 (Oct. 2018), p. 022016. DOI: 10.1088/1757-899X/421/2/022016 (cit. on p. 40).
- [14] Robyn Jackey, Michael Saginaw, Pravesh Sanghvi, Javier Gazzarri, Tarun Huria, and Massimo Ceraolo. «Battery model parameter estimation using a layered technique: an example using a lithium iron phosphate cell». In: *SAE Technical Paper* 2 (2013), pp. 1–14 (cit. on pp. 44, 47).
- [15] Qiaohua Fang, Xuezhe Wei, Tianyi Lu, Haifeng Dai, and Jiangong Zhu. «A State of Health Estimation Method for Lithium-Ion Batteries Based on Voltage Relaxation Model». In: *Energies* 12 (Apr. 2019), p. 1349. DOI: 10.3390/en12071349 (cit. on p. 47).
- [16] Mathworks. *Simulink Design Optimization User GUide*. 2022. URL: https://it.mathworks.com/help/pdf_doc/sldo/sldo_ug.pdf (cit. on p. 52).
- [17] Maryam Yazdanpour, Peyman Taheri, Abraham Mansouri, and Ben Schweitzer| «A circuit-based approach for electro-thermal modeling of lithium-ion batteries». In: *2016 32nd Thermal Measurement, Modeling & Management Symposium (SEMI-THERM)*. IEEE. 2016, pp. 113–127 (cit. on p. 53).

BIBLIOGRAPHY

- [18] Chao Huang, Zhenhua Wang, Zihan Zhao, Long Wang, Chun Sing Lai, and Dong Wang. «Robustness Evaluation of Extended and Unscented Kalman Filter for Battery State of Charge Estimation». In: *IEEE Access* 6 (2018), pp. 27617–27628. DOI: 10.1109/ACCESS.2018.2833858 (cit. on p. 65).
- [19] Victor M Moreno and Alberto Pigazo. «Kalman filter: recent advances and applications». In: (2009) (cit. on p. 66).
- [20] M Sanjeev Arulampalam, Simon Maskell, Neil Gordon, and Tim Clapp. «A tutorial on particle filters for online nonlinear/non-Gaussian Bayesian tracking». In: *IEEE Transactions on signal processing* 50.2 (2002), pp. 174–188 (cit. on p. 66).